PHYSICAL REVIEW FLUIDS **2**, 100506 (2017)

Near wall turbulence: An experimental view

Michel Stanislas*
Ecole Centrale de Lille, Cité Scientifique, 59655 Villeneuve d'Ascq, France
(Received 19 June 2017; published 17 October 2017)

The present paper draws upon the experience of the author to illustrate the potential of advanced optical metrology for understanding near-wall-turbulence physics. First the canonical flat plate boundary layer problem is addressed, initially very near to the wall and then in the outer region when the Reynolds number is high enough to generate an outer turbulence peak. The coherent structure organization is examined in detail with the help of stereoscopic particle image velocimetry (PIV). Then the case of a turbulent boundary layer subjected to a mild adverse pressure gradient is considered. The results obtained show the great potential of a joint experimental-numerical approach. The conclusion is that the insight provided by today's optical metrology opens the way for significant improvements in turbulence modeling in upcoming years.

DOI: 10.1103/PhysRevFluids.2.100506

I. INTRODUCTION

Since its discovery about 100 years ago by Prandtl, the boundary layer has been the subject of thousands of papers. The two dimensional (2D) equation governing it,

$$\rho\frac{\partial v_1}{\partial t}+\rho v_1\frac{\partial v_1}{\partial x_1}+\rho v_2\frac{\partial v_1}{\partial x_2}=-\frac{\partial p}{\partial x_1}+\mu\frac{\partial^2 v_1}{\partial x_2^2}, \tag{1}$$

which is based on the hypothesis that the boundary layer thickness is small compared to a characteristic length scale of the whole flow, is significantly simpler than the full Navier-Stokes equations. It nevertheless still contains two nonlinear terms, $\rho v_1\frac{\partial v_1}{\partial x_1}+\rho v_2\frac{\partial v_1}{\partial x_2}$, which have made a fully theoretical approach out of reach since Prandtl's discovery.

When the Reynolds number is high enough, because of these nonlinear terms, this boundary layer becomes turbulent. Based on Eq. (1) and freezing time, it looks like the visualization shown in Fig. 1, obtained with a laser light sheet and smoke.

As illustrated by this image, turbulence is three dimensional and multiscale, and it is also unsteady. To try to model it in practical situations, it is usual to extract the Reynolds-averaged equation from the above equation (1):

$$\rho\overline{v}_1\frac{\partial\overline{v}_1}{\partial x_1}+\rho\overline{v}_2\frac{\partial\overline{v}_1}{\partial x_2}=-\frac{\partial\overline{P}}{\partial x_1}+\mu\frac{\partial^2\overline{v}_1}{\partial x_2^2}+\frac{\partial(-\rho\overline{v_1'v_2'})}{\partial x_2}. \tag{2}$$

This does not solve the problem, as a correct modeling in realistic configurations of the last term of this equation is still a riddle for all of us.

Although it would be quite interesting to make a detailed review of the progress in understanding and modeling of near wall turbulence, this would probably fill a book and is not the aim of the present contribution (such a review can be found, for example, in Ref. [1] for experimental data or Ref. [2] for high Reynolds number). The objective here is for the author to make a personal contribution (which will probably bring more questions than answers) based on his own experience of the field in the past 25 years and describe the tracks he tried to follow, more or less successfully, in attempting to bring some understanding to this question. For this reason, the author must apologize in advance

*michel.stanislas@ec-lille.fr

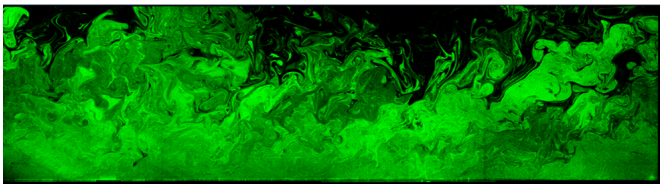

FIG. 1. Instantaneous visualization of a turbulent boundary layer at high Reynolds number using smoke and a YAG laser light sheet.

to all the people who have contributed to this field of turbulent boundary layers (TBL) and are not cited in the present limited contribution.

At the start of such a quest, it is of interest to ask ourselves what we know. Of course, we could then begin by writing a few hundred pages, but this is again not the author's aim. We can try, with subjectivity of course, to extract a few facts which seem of importance to guide the quest.

The first crucial characteristic of a turbulent boundary layer is well illustrated by Fig. 2. The turbulence intensity, as measured by hot wire anemometry (HWA) by several authors, is high and anisotropic over most of the boundary layer (BL) thickness and is maximum very close to the wall. From an experimental point of view, this is an extremely difficult challenge which is not yet solved, even with the smallest probes [3] or the biggest wind tunnels [4]. The near-wall-turbulence peaks are often beyond the best possible spatial resolution, especially when increasing the Reynolds number.

The second difficulty researchers had to face is that near wall turbulence is not just a random process which can be looked at statistically. The key contributions to the understanding of this fact should be attributed to Ref. [9], which was the first to presume the existence of horseshoe vortices in the TBL (see Fig. 3) and to Ref. [10], which was the first to visualize near wall streaks, as shown in Fig. 4.

Such an organization is a great modeling problem, as Reynolds averaging erases it completely. A relative understanding of it has developed rapidly. Streaks have been separated into low (LSS) and high (HSS) speeds, parallel to each other and alternating in span [10]. Ejection of low-speed fluid away from the wall and sweeps of high-speed fluid toward the wall were identified [11–14]. Based on these observations, various models of a "near wall organization" were proposed at different stages, exemplified by Fig. 5 from Ref. [15], which shows low-speed streaks (LSS) lifted up by streamwise vortices. This ended on the near wall cycle proposed in Ref. [16]. Besides, studies were performed

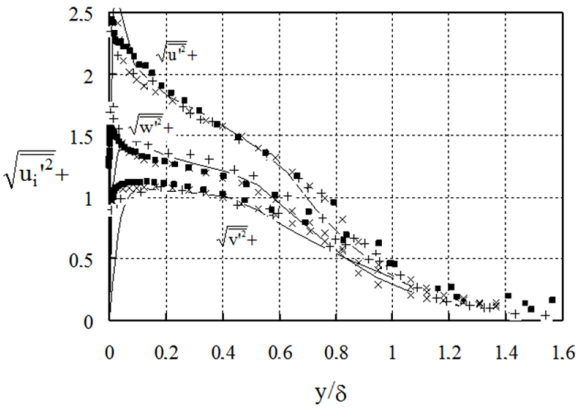

FIG. 2. Turbulence intensity components in a flat plate turbulent boundary layer, obtained from HWA. ■ $Re_\theta = 20\,800$, Carlier and Stanislas [5]; + Klebanof [6], × Erm and Joubert [7], and DNS Spalart [8].

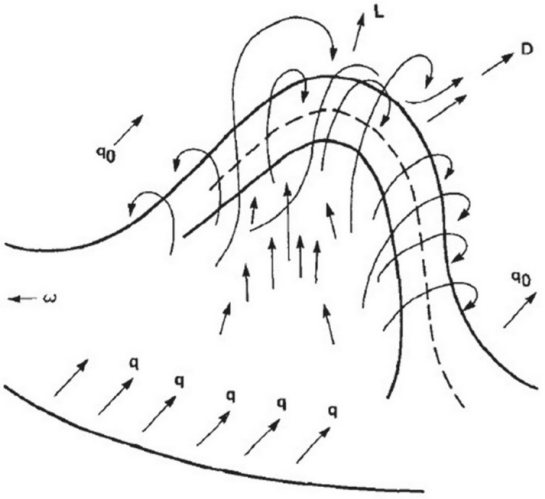

FIG. 3. Horseshoe vortex model of Theodorsen reproduced from Ref. [9].

on the organization further away from the wall, well summarized in Ref. [17], as illustrated in Fig. 6, which describes vortex packets engulfing low-speed fluid.

A relatively recent discovery, which can be attributed initially to Ref. [1] and was confirmed in Ref. [18], is illustrated in Fig. 7: At sufficiently high Reynolds number, a second peak of turbulence grows away from the wall, which is not at all predicted by the existing models. This is an active subject of research which will not be summarized here as it is already dealt with in Refs. [2,19].

Despite this wealth of understanding developed by the turbulence community in the past 50 years, and despite some quite successful models proposed, for example, in Ref. [20], it has not yet been possible to make use of this wall turbulence organization to improve any near-wall-turbulence model.

All the above findings were done in the canonical zero pressure gradient (or flat plate) TBL. When a pressure gradient exists, the complexity is tremendously increased, as this pressure gradient can be any function of x_1, positive or negative, increasing or decreasing, which gives an infinite number

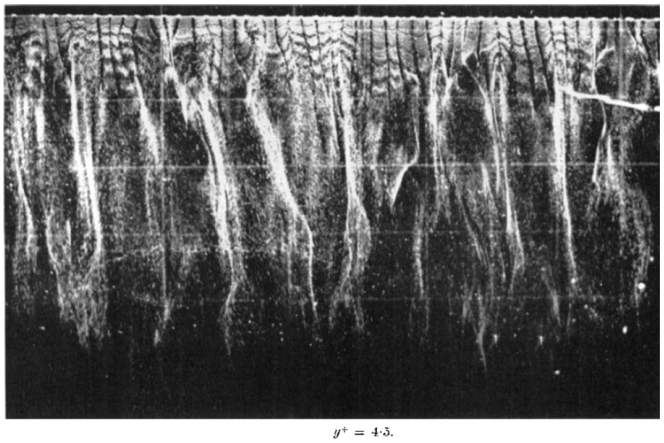

FIG. 4. Near wall streaks visualization using the bubble wire technique by Kline *et al.*, reproduced from Ref. [10].

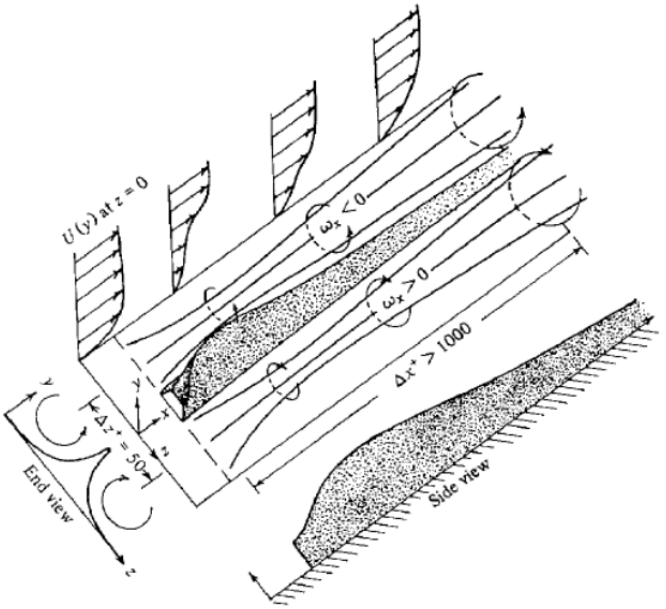

FIG. 5. Model of near wall organization by Blackwelder and Kaplan, reproduced from Ref. [15].

of possibilities. The most classical case, exemplified by Fig. 8, is the flow on the suction side of an airfoil in cruise conditions where, to generate lift, the fluid has to accelerate and decelerate, leading to a negative/favorable pressure gradient (FPG) followed by a positive/adverse pressure gradient

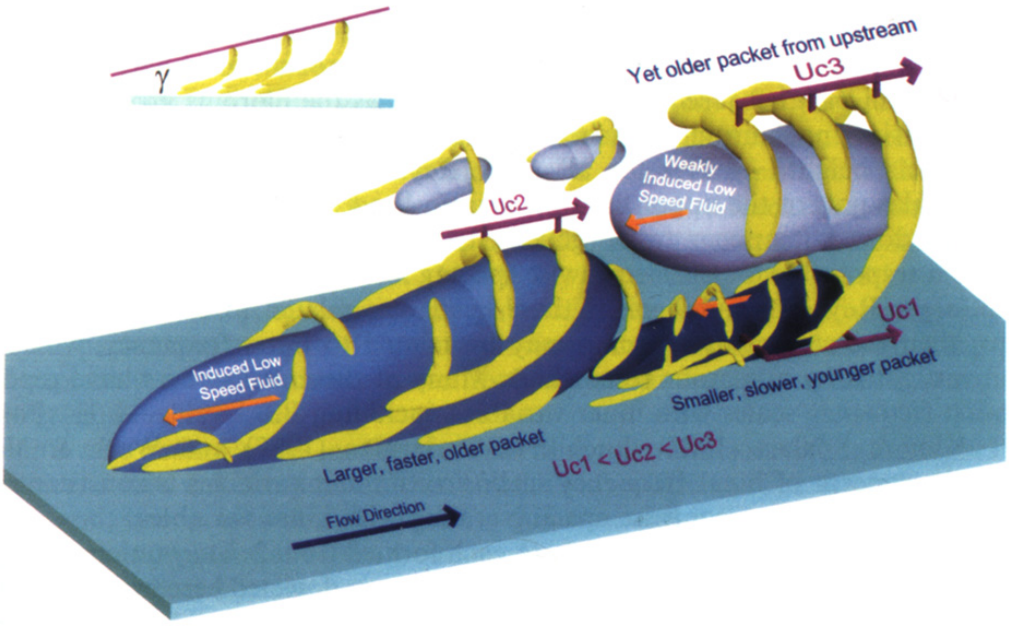

FIG. 6. Model of hairpin packets of Adrian, reproduced from Ref. [17].

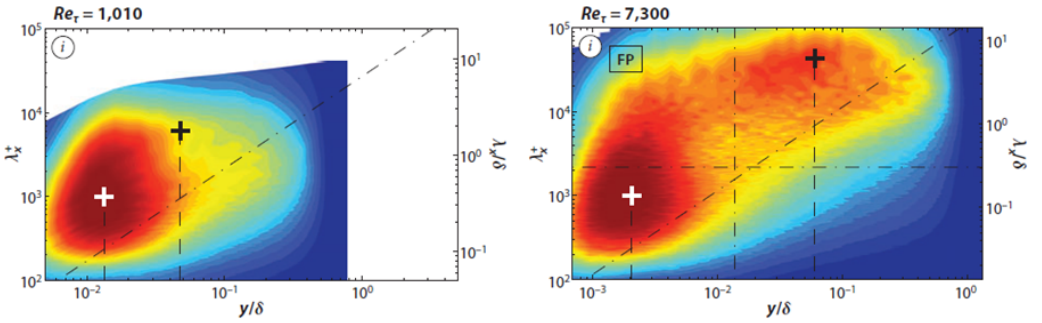

FIG. 7. Premultiplied spectra as a function of wavelength and wall distance at two Reynolds numbers showing the development of the outer turbulence peak when the Reynolds number increases, reproduced from Ref. [21].

(APG) applied to the boundary layer. The shape of the pressure gradient is, of course, directly linked to the shape of the airfoil suction wall and it is the APG part which represents the present modeling challenge. Because of this complexity and the lack of experimental means, little has been done until very recently on the organization of APG TBL turbulence. But, on the theoretical point of view, some advances were possible, well represented by Refs. [22,23].

The breakthrough which appeared in the past 10–15 years and which created a revolution in turbulence research is the tremendous development of digital particle image velocimetry (PIV) [24], allowing us to look at the spatial structure of flows with large fields, good spatial resolution, and enough samples to perform converged statistics, even on coherent structures. This, compared with hot wire anemometry (HWA), even with several probes, provides incomparable data on the spatial organization of the flow. This fact is well illustrated by Fig. 9 from Ref. [25], which gives the streamwise velocity fluctuations in a flat-plate TBL and which should be compared to Fig. 1, a smoke visualization of the same flow.

The flow structure is still in the PIV data but now visible down to the wall and both a length scales and velocity scales of the coherent motions (which are the building blocks of theory in fluid mechanics) can be extracted. What will be attempted here is to illustrate the potential of this approach which, at the time scale of basic research, is in its initial stage, and which will surely trigger some theoretical breakthrough, just as hot wire anemometry did when it became available (remember Kolmogorov).

II. AVAILABLE TOOLS

To perform experiments in fluid mechanics, two essential tools are needed: a wind (or water) tunnel and an adequate measurement technique.

As far as the wind tunnel is concerned, if high-Reynolds-number boundary layers are targeted, they are usually obtained by increasing the velocity. This limits the size of the facility but raises serious problems of spatial resolution of the measurements. Another solution is to play with the fluid properties, like the pressure level as in Princeton superpipe, for example [26]. A few teams around the world have tried to use the length scale, leading to fairly large facilities such as the ones

FIG. 8. Sketch of the flow over an airfoil at low angle of attack emphasizing the TBL in the APG region on the suction side.

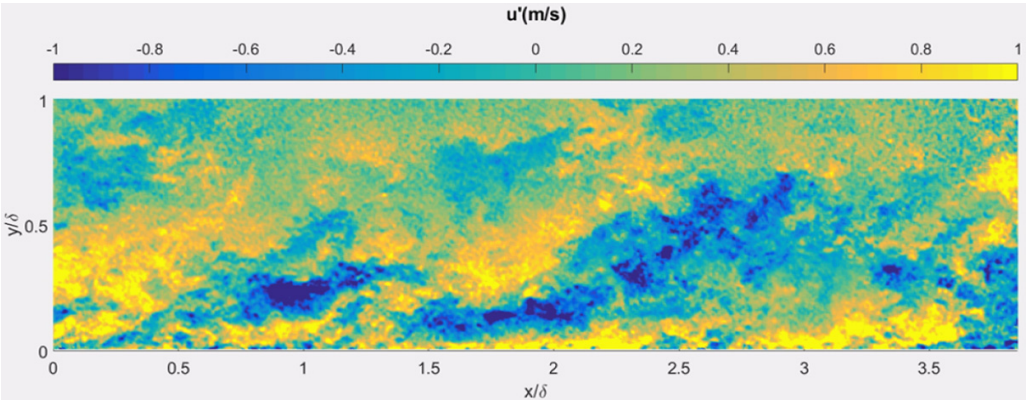

FIG. 9. Instantaneous map of the streamwise velocity fluctuations in a high-Reynolds-number turbulent boundary layer [25].

in Melbourne [27] and New Hampshire [4]. The wind tunnel that the author has built in Lille is of this last category [5]. A photograph is provided in Fig. 10. The test section is 21 m long and is now transparent on all sides, providing full optical access along the whole test section. The cross section is 2 m wide and 1 m high with a free-stream velocity range from 1 to 10 m/s. The free-stream velocity is regulated within 0.5% and the temperature within 0.15 °C.

Such a facility allows us to reach Reynolds numbers Re_θ based on the momentum thickness of the order of 20 000 with a boundary layer thickness of the order of 30 cm. With such a scale, good resolution can be obtained very near to the wall, both with classical techniques such as hot wire anemometry or with optical techniques like PIV.

Looking at the measurement techniques, if the hot wire anemometer is still unbeatable in terms of spectral range, it encounters a lot of difficulties when coming very close to the wall and it can hardly give spatial information (hot wire rakes are heavy to operate). In the past 20 years, optical metrology has brought a revolution in fluid mechanics measurement with the still ongoing development of particle image velocimetry. It is not possible to present here all the developments and possibilities of PIV, but a good synthesis is available in Ref. [28]. Stereo-PIV measurements of the three components of the velocity in a plane with a field of view of the order of 200×200 mm^2 and a spatial resolution of the order of 1×1 mm^2 can be considered presently as a standard. As will be shown in the following, it is now quite easy to combine several cameras to increase the field of view without losing spatial resolution. As the sensitivity of the cameras has dramatically increased in the past

FIG. 10. Photo of the boundary layer wind tunnel at Laboratoire de Mécanique de Lille (LML).

10 years, the amount of light needed is much less, allowing us either to enlarge the field of view or to use less powerful lasers. One important limitation can sometimes be the beam quality of the compact lasers generally sold with PIV systems, which do not allow us to make thin light sheets on large fields. The development of high-speed cameras and high-repetition lasers allows stereo-PIV to be performed today in a typical field of view of the order of 100×100 mm^2, with the same spatial resolution as above and a repetition rate of a few kHz. Two known limitations of this last approach are the output power of the high-repetition lasers and the size of the pixels of the high-repetition cameras. Both should improve continuously in the future. The rapid development in recent years of tomo-PIV [29] should be mentioned as a nice perspective for quantitative characterization of the three-dimensional (3D) aspects of structures in turbulence, especially with the recently proposed shake-the-box algorithm [30]. The work presented in the following uses mostly stereo-PIV or two-components (2C) PIV, sometimes combined with other techniques to compensate for the low sampling rate of standard PIV (typically less than 10 Hz). No doubt the subject of boundary layer structure will continue to be explored in the near future using these recent developments of the PIV technique.

III. FLAT PLATE BOUNDARY LAYER

As was explained earlier, setting the pressure gradient to zero in Eqs. (1) or (2) greatly simplifies the theoretical approach. Nevertheless, Eq. (2), although being parabolic, needs a turbulence model for the $\frac{\partial(-\rho\overline{v_1' v_2'})}{\partial x_2}$ term. Such a model was proposed by Prandtl in 1921 as the "mixing length" hypothesis, leading to the well-known logarithmic region κ constant whose value is still today a subject of controversy [31,32]. Even the most advanced $k-\epsilon$ or full Reynolds stress models contain a significant number of unknown terms which are crudely modeled and of arbitrary constants which are tuned on experimental data. (One can easily be convinced of the amount of arbitrariness in turbulence modeling by looking at the modeled transport equation for the turbulence dissipation ϵ.) One key issue in turbulent boundary layers is that it has not yet been possible to find a universal representation of them in their entirety. Two scalings are needed (one inner and one outer), which means that there is a continuous change between two physics when moving from the wall outward. It is only in the overlap region between these two physics (which is a small percentage of the boundary layer thickness) and in the thin viscous layer attached to the wall that a real theory has been found for the mean velocity. All the rest (80 to 90%) is empirical.

The internal organization of near wall turbulence has been the subject of considerable attention since the 1950s. Until recently, apart from direct numerical simulation (DNS), these studies were mostly based on visualizations and spatial correlation of hot wire signals. Although they have brought a lot of understanding [33], they were mostly qualitative and limited to the near wall region and low Reynolds numbers. It is PIV, with for example, the pioneering work of Ref. [17], which brought a quantitative field information, as mentioned earlier, with both length scales and velocity scales characterizing the coherent structures observed in the flow. It is only very recently that technical progress on cameras and computers has allowed us to build sufficiently converged statistics from PIV data. The following material will try to illustrate this approach, looking first at the near wall region, which is already quite universal at moderate Reynolds number, and then at the outer part where a sufficiently large Reynolds number is needed to evidence large-scale structures [19].

The question of the zero pressure gradient (ZPG) should be addressed here. In theory, $\partial p/\partial x_1$ should be exactly zero. In practice, this implies tuning the wind tunnel walls with a slight divergence (to take into account the growth of the BL on them), which is complicated, expensive, and not very stable in time. Some researchers, including the author, work with a wind tunnel of constant cross section. This imposes a slight constant pressure gradient on the BL, which is then called a flat plate and not a ZPG BL to make the distinction clear. It has been noted very early that the near wall scaling is common to ZPG and FP BL, rectangular channel and circular pipe flows. The corresponding physics (that is, the turbulence organization) is then common too. Of course, the outer

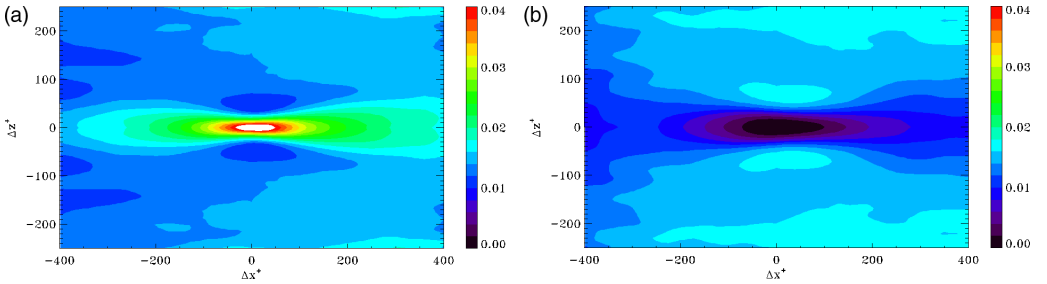

FIG. 11. Correlation in a plane parallel to the wall between the low-speed streaks and the ejections (left) or sweeps (right), reproduced from Ref. [35].

part is significantly different between the three types of flow (BL, channel, and pipe) [34]. It is not known yet if the outer turbulence organization differs between the ZPG and FP BL, but they look very similar.

A. Near wall organisation

The potential of PIV in terms of analysis of the turbulence structure is well illustrated by the work of Lin [35,36]. A stereo-PIV experiment was performed in 10 planes parallel to the wall, spaced by 4 wall units in the wall-normal direction and localized in the buffer layer (between $y^+ = 14.5$ and 50) of a flat plate turbulent boundary layer at $\mathrm{Re}_\theta = 7800$. At that time, due to the storage capacity, only 500 PIV samples per plane could be recorded. After a careful validation of the data by comparison with hot wire anemometry, it was possible to transpose the digital image analysis approach to the fields of turbulence fluctuations. For that purpose, a scalar detection function had to be defined which is representative of the coherent structure to be extracted (low- or high-speed streaks; ejection; sweep; vortex). From this detection function, a binary indicative function can be built, generally by thresholding. Following this, some noise filtering has to be applied, usually by convolution filters, to provide a set of objects which can be numbered and measured. They can also be used as masks on the velocity fields to characterize the turbulence fluctuations inside them.

Finally, spatial correlation between indicative functions of different structures can be performed to provide a statistical estimation of their relative positions (all the details are in Ref. [35], which has a French title but is written in English). The results of such spatial correlations are quite interesting, as illustrated by Figs. 11–14.

Figure 11 provides the spatial correlation between low-speed streaks and ejections (left) and sweeps (right) respectively at $y^+ = 14.5$, which is the plane closest to the wall. The results clearly confirm statistically what is already known from early work: Ejections are inside the low-speed streaks while sweeps are outside.

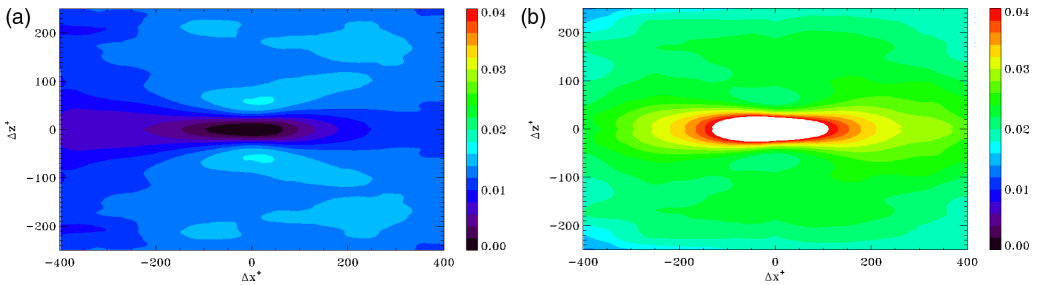

FIG. 12. Correlation in a plane parallel to the wall between the high-speed streaks and the ejections (left) or sweeps (right), reproduced from Ref. [35].

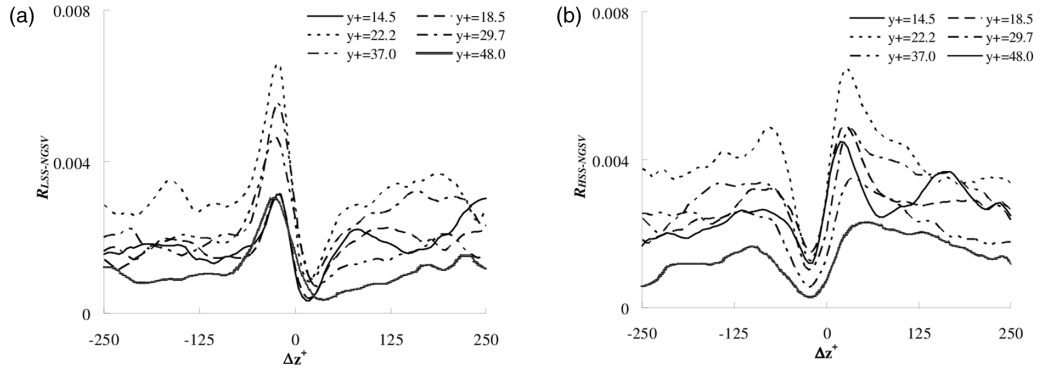

FIG. 13. Correlation at different wall distances between the low-speed streaks and the negative vortices (left) and between the high-speed streaks and the same negative vortices (right), reproduced from Ref. [35].

Figure 12 then provides the spatial correlation between high-speed streaks and ejections (left) and sweep (right) respectively at $y^+ = 14.5$. Here also, the fact that sweeps are inside the high-speed streaks while ejections are outside is clearly confirmed statistically with a full spatial information. When we compare Figs. 11 (left) and 12 (right), sweeps appear more localized in HSS than ejections in LSS.

It is then possible to look at the respective positions of streaks and streamwise vortices. This is done in Fig. 13 at different wall distances and as a function of the spanwise coordinate z. A dominant side is observed, which is inverted if the sign of the vortex is changed. If streamwise vortices can be found on both sides of a streak, there is statistically a dominant side depending on the type of streak (low or high speed) and on the sign of the vortex. This is clear proof of organization.

The same analysis can be performed on the relations among ejections, sweeps, and streamwise vortices. The result is given in Fig. 14, which shows that in the buffer layer, ejections, and sweeps are very strongly linked to the streamwise vortices. Again, a symmetric figure is obtained for the positive vortices.

Based on these spatial correlation analyses and on measurement of different characteristic parameters of the structures (size, orientation, etc.), it was possible, from the work of Ref. [35], to build a quantitative sketch of the coherent structures organisation in the buffer layer, which is displayed in Fig. 15. The first thing to note in this sketch is that the spacing and size of the streaks is in good agreement with the literature [37]. Then, it is remarkable that vortices appear relatively short in length (about 100 wall units, WU), directly generating an ejection and a sweep on the

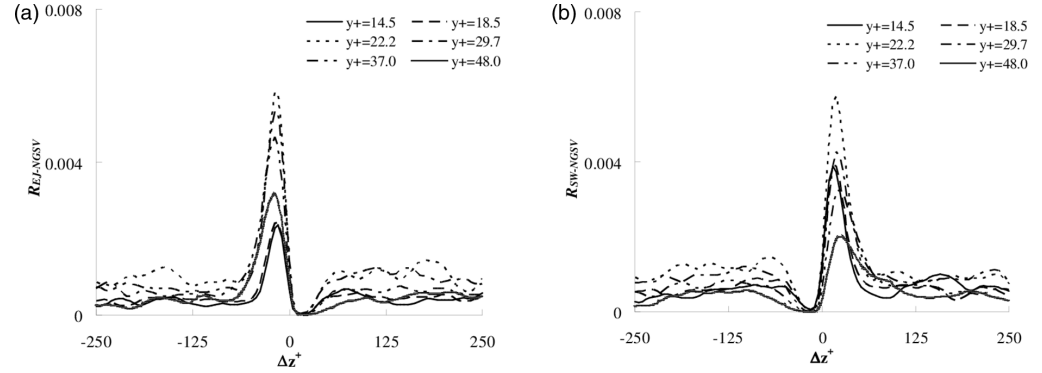

FIG. 14. Correlation at different wall distances between the ejections and the negative vortices (left) and between the sweeps and the same negative vortices (right), reproduced from Ref. [35].

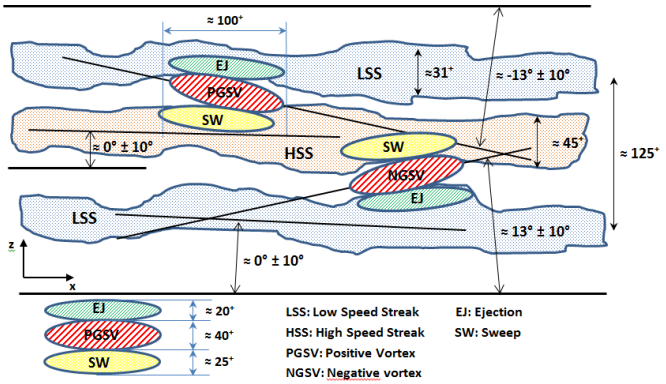

FIG. 15. Model of very near wall organization in a plane parallel to the wall below $y^+ = 50$.

sides corresponding to their sign and positioning themselves between adjacent streaks so that the ejection is in the low-speed streak and the sweep in the high-speed one. It is also noticeable that these vortices are not really streamwise but show a mean spanwise angle, and the sign depends on the vortex sign. What is not shown in this figure, but was observed in the study, is that these vortices have a maximum frequency of appearance at $y^+ \simeq 20$ with a radius of the order of 20 WU. This is about 10 Kolmogorov length scales, which was also found in Ref. [38] to be a universal size of the vortices up to the top of the log layer.

In the existing literature, the sketch of Fig. 15 bears a striking resemblance to the model developed in Ref. [39] from a stability analysis of the streaks and presented in Fig. 16. The conclusion is that there is a clear mechanism of production of quasistreamwise individual vortices on the sides of the low-speed streaks, due to a sinuous instability of these streaks [40]. This phenomenon seems to be bound to the buffer layer where the mean velocity gradient is strong enough to generate instabilities of the instantaneous velocity profiles and where the viscosity effects are low enough to let these instabilities develop.

This is somehow confirmed by Fig. 17 extracted from a DNS of plane channel flow in Ref. [41]. The low-speed streaks are visualized in yellow. The vortices are evidenced using a Q criteria and are colored in blue if they are below $y^+ = 50$ and in red above this wall distance. As can be seen, below $y^+ = 50$ most vortices are individual and quasistreamwise while above a much wider range of orientation is observed.

In fact, the work in Ref. [35] also permitted the identification of pairs of counter-rotating vortices surrounding low-speed streaks, but in much less number than the preceding individual ones. These counter-rotating pairs are usually considered as the legs of the horseshoe vortex [9] or hairpin

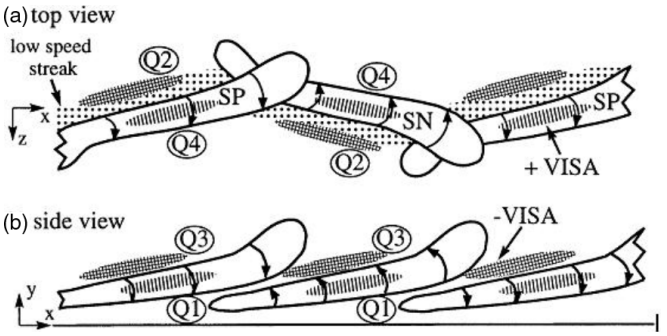

FIG. 16. Model of Schoppa and Hussain, reproduced from Ref. [39].

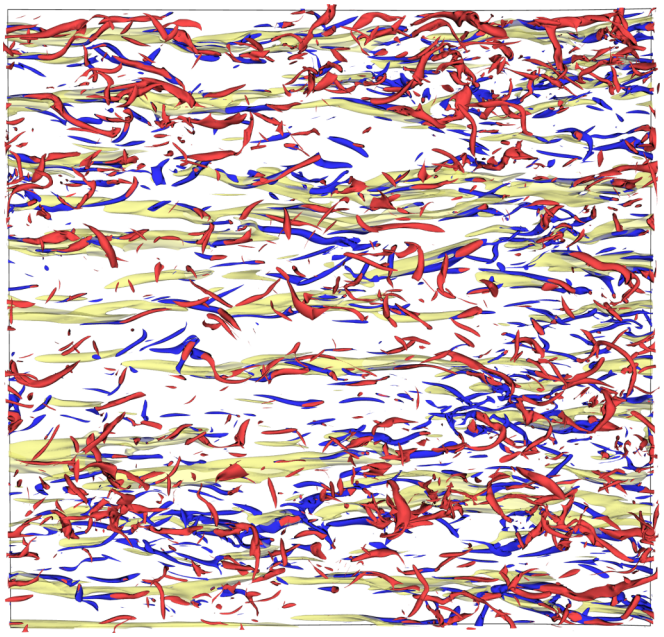

FIG. 17. Visualisation of streaks (yellow), vortices below $y+ = 50$ (blue), and vortices above $y+ = 50$ (red) in a DNS of channel flow at Re $= 600$ from [65] (2009).

vortex [42]. It has its origin in a effectively varicous of the same low-speed streaks associated with the well-known lift and ejection of low-speed fluid away from the wall [10]. Roughly, at the Reynolds number in Ref. [35] ($\mathrm{Re}_\theta = 7800$), about 80% of the vortices detected were from sinuous instability origin and about 20% from varicous.

Based on the above observations, it is possible to propose a scenario of organization in the near wall region, which is sketched in Fig. 18. The vortices are generated by two types of instabilities of the meandering low-speed streaks and appear close to the wall, in a quasistreamwise cane shape,

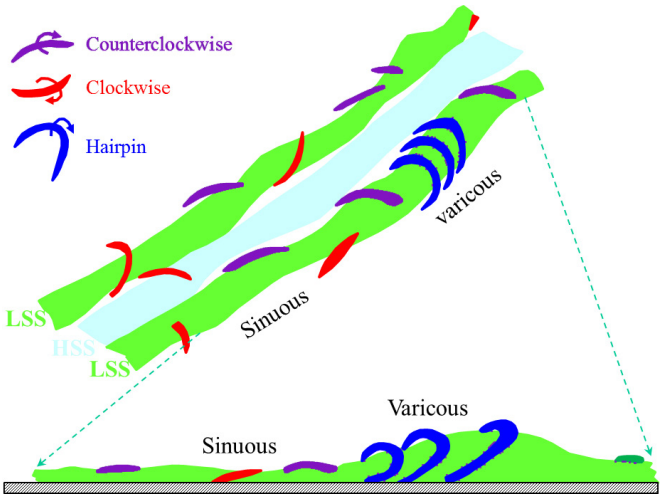

FIG. 18. Model of near wall organization.

between nearby low- and high-speed streaks if they originate from the sinuous instability and as hairpins, riding a lifting low-speed streak, if they come from the varicous instability. Such a scenario explains some previous observations: the fact that most vortices observed above the buffer layer are canes [5,38] and the fact that a non-negligible number of vortices rotating against the natural vorticity of the mean flow are observed in a wall-normal streamwise plan [5,43]. It is also clear now that the hairpin vortices were much easier to observe in the early visualization studies than the quasistreamwise ones as these last one, which originate from the sinuous instability of the streaks, are much closer to the wall.

B. Outer organization

As was indicated in the introduction, a new turbulence activity develops in the outer part of wall turbulence (boundary layers, channels, and pipes) when the Reynolds number increases, with a clear outer peak (or plateau) of turbulent kinetic energy [18]. This peak seems to be linked to the large- and very-large-scale motions identified in the outer layer in Ref. [44], which are active subjects of investigation [19,45,46]. The difficulty in such a situation is to have both a very large field of view in the streamwise direction to capture these structures and a good enough spatial resolution to characterize them. This is very difficult to do with only PIV, although the next section will show that the considerable progress of the equipment improves the prospects. When the technique sets the limits of one measurement method, it is often possible to combine the advantages of different methods and of some adequate mathematical tools to solve the problem. This is what was done in an original experiment performed in the frame of the WALLTURB European project [47]. It was performed in the LML Boundary Layer Wind Tunnel by a team from LML, the PPRIME Poitiers laboratory, and the University of Chalmers. The interest of the facility is that high Reynolds numbers are obtained by the length scale, which allows a good spatial resolution inside the BL. Combined measurements using a stereo-PIV plane orthogonal to the flow and a rake of 143 hot wires just behind it were performed with a square field of view of the size of the BL thickness (all details are in Ref. [47]). The PIV data had good spatial resolution (2×2 mm^2 for a field of view of 300×300 mm^2) and three velocity components at a low sampling frequency (4 Hz). The hot wire signals were sparsely distributed in the plane and provided only the streamwise component of the velocity, but they were time resolved (30 kHz). In the framework of the thesis by Dekou [48,49], these data were used together with the linear stochastic estimation approach introduced in turbulence by Ref. [50]. Based on this method, it was possible to reconstruct three-component velocity fields in the PIV plane, time resolved at a frequency of 2 kHz and for two Reynolds numbers: $\mathrm{Re}_\theta = 9\ 830$ and 19 660.

Once a velocity field is available, it is possible to process it in the same way as what was done near the wall to extract coherent structures. This was performed by Ref. [48] to characterize low- and high-momentum regions as well as vortical motions. It should be noted here that a terminology different from the near wall region is used to avoid ambiguity. Figure 19 gives an example of reconstruction from the LSE data of the structures identified in one realization. As can be seen, here also vortical motions develop themselves between the low- and high-momentum regions and with a position depending on their sign. Again, this instantaneous fact can be confirmed statistically by computing the spatial correlation between the indicative functions of the different structures. An example of such correlations between positive vortical motions and respectively low- and high-momentum regions is given in Fig. 20.

Based on these spatial correlations and on the size measurement of the different indicative functions, it is possible, as in the near wall region, to build a quantitative sketch of the organization in the outer part. This sketch is given in Fig. 21. A strong similarity is observed between this organization and the near wall one of Fig. 15. Quasistreamwise vortical motions develop between low- and high-momentum regions and tend to lift the LMR and bring HMR toward the wall. Like the vortices near the wall, these vortical motions are not always paired (see Fig. 19). Globally, a strong analogy can be made with earlier sketches of the near wall organization such as the one

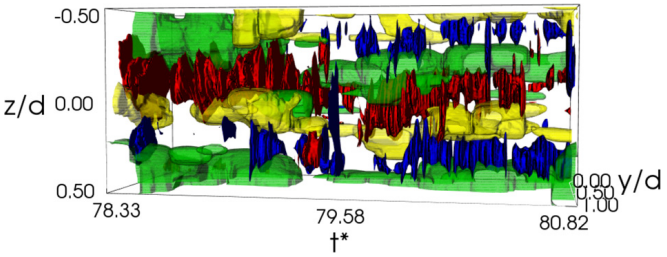

FIG. 19. Spatial organization of coherent structures obtained by Dekou *et al.*, reproduced from Ref. [49]. Positive and negative vortices are highlighted in red and blue respectively while low- and high-momentum regions are highlighted in green and yellow respectively.

of Ref. [15] given in Fig. 5. But, as shown in Fig. 21, the scaling is different and based now on outer variables (see Ref. [48] for details). In fact, what is reconstructed by the LSE is not the exact instantaneous flow structure, especially inside the vortical motions which (based on DNS [51]) are known to be constituted of many smaller vortices. It should be remembered here that LSE is based on statistical operators: the spatial correlations between the hot wire and PIV signals. Therefore, what is reconstructed is an averaged view based on the instantaneous hot wire signals. LSE is consequently bringing out a simplified picture of the flow which is statistically representative and which can be used as a simple model of the outer organization. This brings us to a quite simple model of the BL organization based on two similar systems of staggered low- and high-speed motions, with vortical motions in between. The two systems of Figs. 18 and 21 are one above the other, one with inner and the other with outer scaling.

C. Cross-talk between inner and outer systems

Having identified two organizations at two different scales, the interesting question which follows is that of the interaction of the two systems. This question has been addressed for a long time and by many researchers. The action of the outer system on the inner one was recently modeled in Ref. [20]. It can also be illustrated by the work of Ref. [52], which looked at the space-time correlation between the pressure fluctuations and the velocity field in a high-Reynolds-number flat plate boundary layer. Figure 22, from this study, gives a plot of the space-time correlation coefficient Rpu between the wall pressure fluctuations and the streamwise component of the fluctuating velocity. Time is scaled with the external velocity Ue and the boundary layer thickness δ. Distinction is made in this

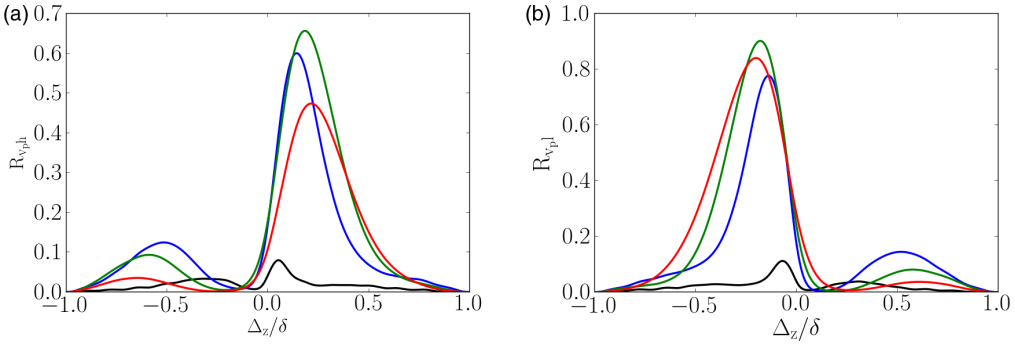

FIG. 20. Spanwise correlation of the positive vortical motions and the low-momentum regions (left), the high-momentum regions (right) plotted at different wall-normal positions at Re = 9830, reproduced from Ref. [49]. Black, 0.037δ; blue, 0.14δ; green, 0.27δ; and red, 0.55δ.

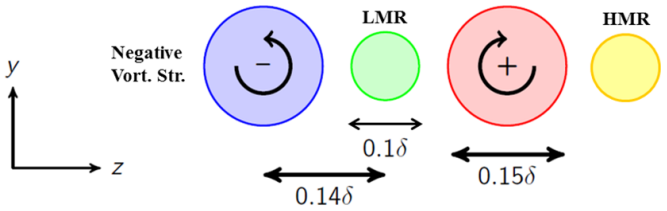

FIG. 21. Model of outer organization of Dekou *et al.*, reproduced from Ref. [49].

figure between positive- and negative-pressure fluctuations. As can be seen, the wall pressure (and consequently the near wall system) is strongly correlated with coherent motions at the scale of the boundary layer thickness in the wall-normal direction and of several δ/Ue in time.

Looking at the correlation of $p > 0$ with the three components of the velocity fluctuations, as illustrated in Fig. 23, gives a clear indication that the main part of the interaction is with the front part of large sweeping motions toward the wall. For $p < 0$, it is more the rear part of the same large sweeping motion (see Fig. 22).

The action of the inner system on the outer one is well illustrated by Fig. 24, also from Ref. [52], which gives now the correlation between the field pressure fluctuation at y_p and the streamwise component of the velocity fluctuation for three increasing Reynolds numbers. As can be observed, an elongated structure appears at a shallow angle to the wall, with a time extension increasing with Reynolds number to reach more than $6.\delta/Ue$ at the highest Reynolds number. This elongated structure does not appear in Fig. 22 for the wall pressure. It is most probably linked to the large scale motions identified in Ref. [17], which have their origin in the varicous instabilities of the streaks.

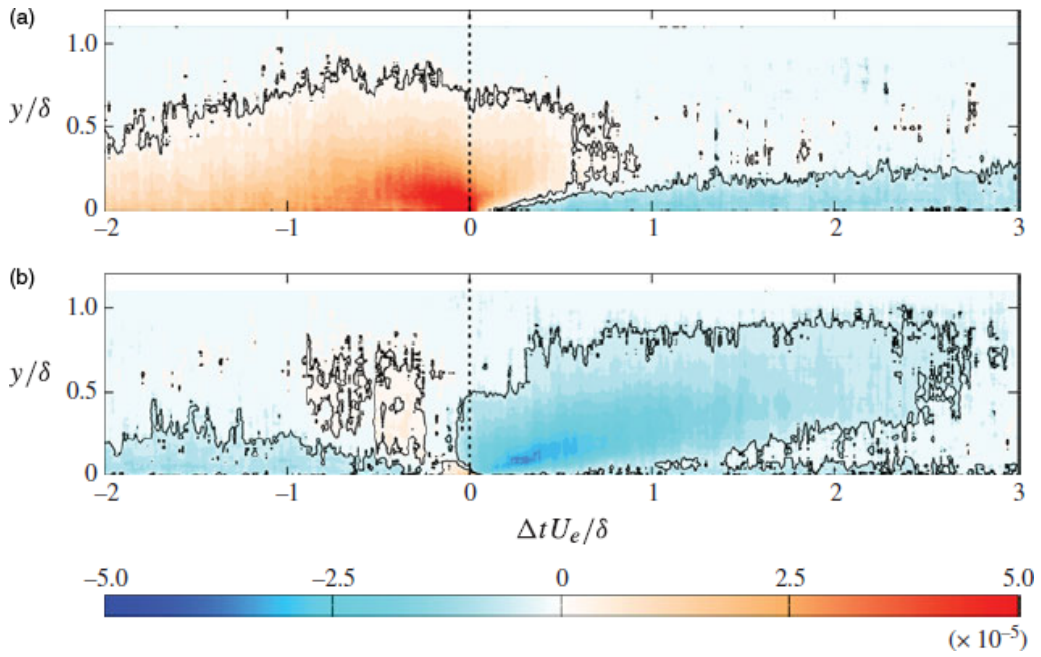

FIG. 22. Cuts of the wall pressure and streamwise velocity fluctuation correlation Rpu in the $\Delta t\,y$ plane at $z/\delta = 0$ and at $\mathrm{Re}_\theta = 10\,000$ with (a) $p > 0$ and (b) $p < 0$. Reproduced from Ref. [52].

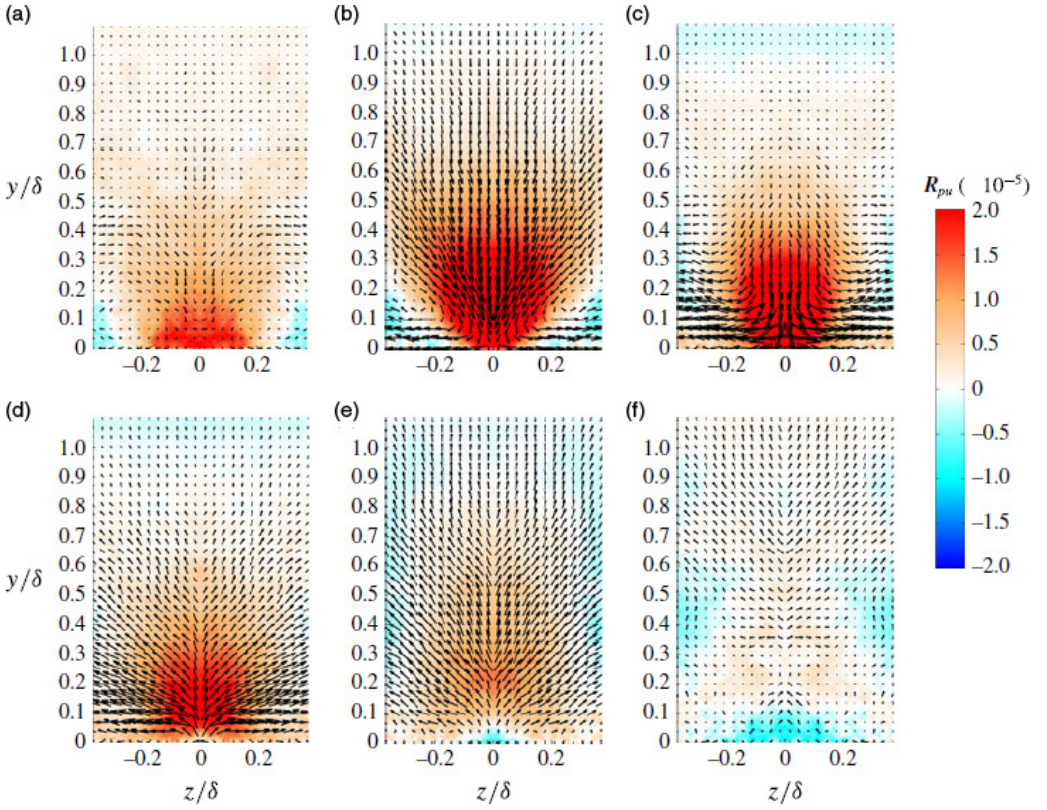

FIG. 23. Cuts of the Rpu, Rpv, Rpw wall pressure and velocity fluctuations correlations in the zy plane at (a) $\Delta t/Ue = -1.46$, (b) $\Delta t/Ue = -0.46$, (c) $\Delta t/Ue = 0.00$, (d) $\Delta t/Ue = 0.16$, (e) $\Delta t/Ue = 0.36$, and (f) $\Delta t/Ue = 0.96$ and at $\mathrm{Re}_\theta = 10\,000$ with $p > 0$. Reproduced from Ref. [52].

D. Modeling

Based on the evidence of these large outer structures and on the fact shown by several authors that they have a significant streamwise extent [44,46,49,52], the idea came to the authors of Ref. [53] to modify the well-known model of spectrum from Ref. [54] by adding an extra range of wave numbers with a $-m$ slope, different from the -1 slope of Ref. [54], and which should be between 0 and -1, as illustrated in Fig. 25.

By integrating this modeled spectra, it is possible to build a model of the evolution of the streamwise turbulence intensity as a function of wall distance:

$$\tfrac{1}{2}\overline{u'^2}(y)/u_\tau^2 \approx C_{s0} - C_{s1}\ln(\delta/y) - C_{s2}(y/\delta)^{p(1-m)}\mathrm{Re}_\tau^{q(1-m)}, \tag{3}$$

where the first two terms on the right-hand side are the standard [54] terms giving a logarithmic law to the profile in the outer part. The last term of the right-hand side is the one added by the present model, due to the extra range of wavelengths with slope $-m$. In Ref. [53], the model was built based on the Princeton superpipe data [18]. In Ref. [55], a trial was made to extend the generality of the model to boundary layers by applying it to high-Reynolds-number data from different facilities around the world. These facilities are sketched in Fig. 26. They include the boundary layer data [3] in the superpipe, the data from the New Hampshire FPF facility [4], the measurements [27] in the Melbourne HRNBLWT, and finally the data [5] obtained in the Lille LML wind tunnel.

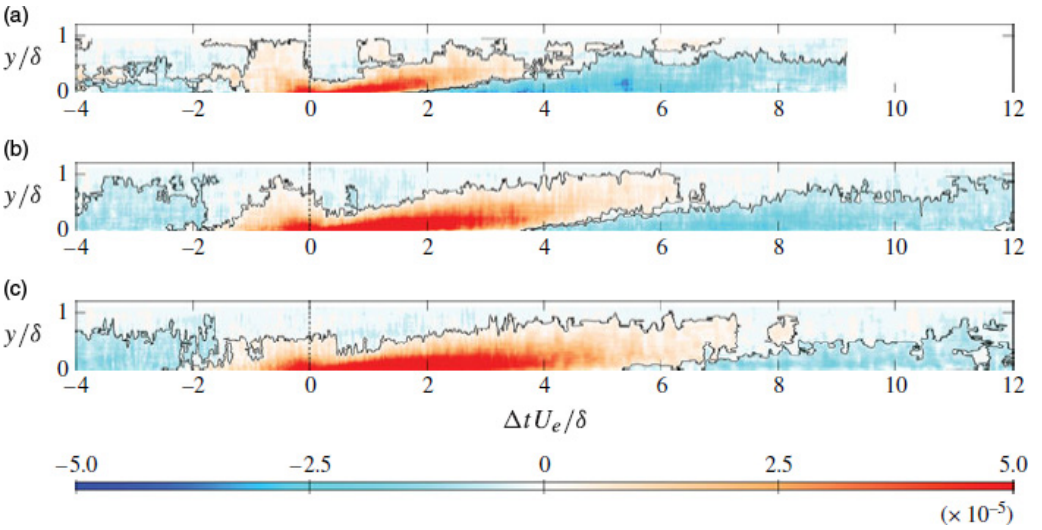

FIG. 24. Cuts of the field pressure and streamwise velocity fluctuation correlation Rpu in the $\Delta t y$ plane at $z/\delta = 0$ and at (a) $\mathrm{Re}_\theta = 7300, {y_p}^+ = 28$, (b) $\mathrm{Re}_\theta = 10\,000, {y_p}^+ = 48$, and (c) $\mathrm{Re}_\theta = 18\,000, {y_p}^+ = 85$. Reproduced from Ref. [52].

The comparison of the proposed model to these four datasets is presented in Fig. 27. As expected, the model of Ref. [54] fits quite well with the logarithmic region in the outer part. The extra range of wave numbers, corresponding to the observed very large scales, allows the representation of the outer peak (or plateau) which develops when increasing the Reynolds number. This relatively good agreement of the model with this range of data enabled the authors of Ref. [55] to propose a set of parameters for their model which could be validated at a much higher Reynolds number by comparison with data measured in the Salt Lake Desert test facility [56,57].

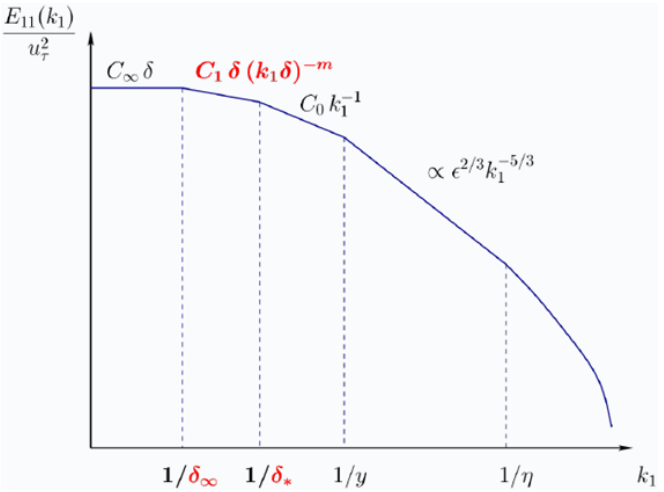

FIG. 25. Model of spectra including an extra range of large scales between $1/\delta_\infty$ and $1/\delta_*$, reproduced from Ref. [53].

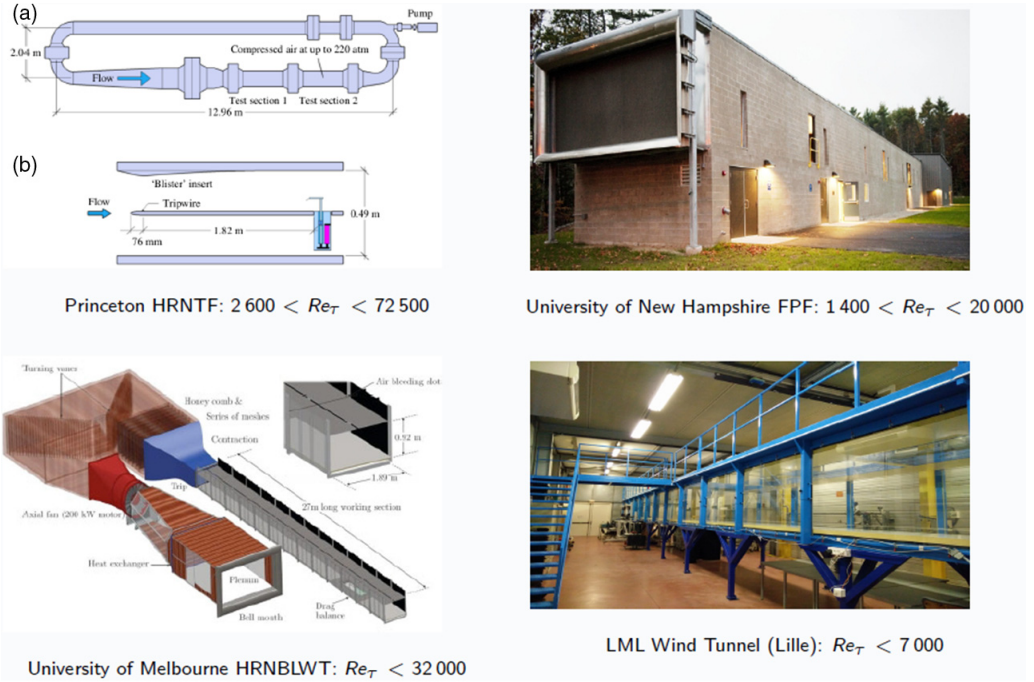

FIG. 26. Set of high-Reynolds-number facilities used in Ref. [55] to validate the model developed by Vassilicos *et al.*, reproduced from Ref. [53].

IV. ADVERSE PRESSURE GRADIENT BOUNDARY LAYER

A. Introduction

All of the above results concern a canonical case, the ZPG (or FP) TBL, which has the advantage of being simpler from the theoretical point of view but is never encountered in practical situations. Usually, not only is the pressure gradient in Eqs. (1) and (2) not zero, but also it is not even constant. It is a function of x_1 which, luckily, is not an unknown but a boundary condition imposed by the outer flow in the case of the boundary layer approximation. Nevertheless, this leads to an infinite number of cases depending on the function chosen for $\frac{\partial p}{\partial x_1}(x_1)$ or $\frac{\partial \overline{p}}{\partial x_1}(x_1)$. Experience has shown that if this pressure gradient is negative (favorable), since the well-known $k-\epsilon$ model [58], turbulence models are not too sensitive and give reasonable predictions. Keeping only the case of positive/adverse pressure gradient (APG), anything is possible between a constant value and any function of x_1 up to a shock wave (this last case being a subject in itself, out of the scope of the present paper). This increases significantly the difficulty of experiments and numerical simulations. The consequence is that for a long time only a few profiles of, predominantly, the streamwise component of the Reynolds stress tensor from a few experiments were available, and nearly no numerical simulations. (The first DNS of adverse pressure gradient (APG) BL was obtained by Spalart [59] in 1993 compared to the one for ZPG by the same author in 1988 [8]. A more detailed one was obtained by Skote [60] in 2002.) The case of a strong adverse pressure gradient is not too difficult, as the boundary layer separates immediately, and nearly any current turbulence model can predict the separation. The case of moderate APG's, without or with separation, is far more challenging for modelers, but, as noted in Ref. [61] and illustrated in Fig. 28, one common physical fact has been observed: the development of a more or less intense second peak of turbulence which, as opposed to the standard near wall peak, spreads and moves away from the wall as it progresses downstream.

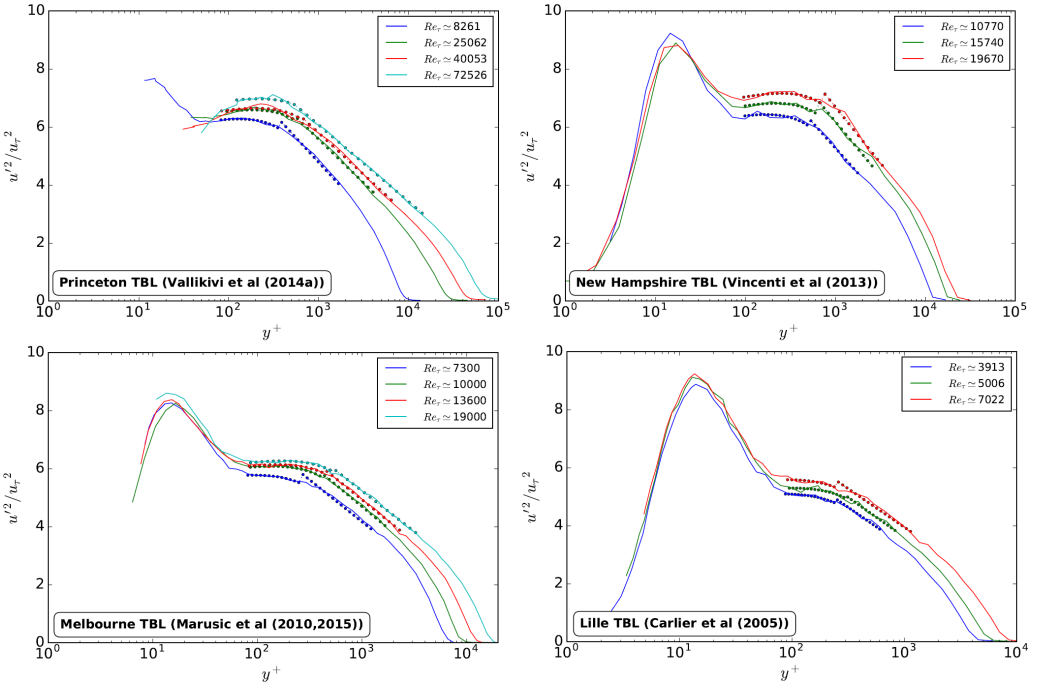

FIG. 27. Streamwise turbulence intensities as a function of wall distance and for different Reynolds numbers. Comparison between the model (symbols) and the experimental data (lines) from the facilities of Fig. 26. Reproduced from Ref. [55].

In that case, as illustrated in Fig. 29 from Ref. [62], even the most advanced turbulence models such as an elliptic blending full Reynolds stress model (EB-RSM) fail to predict correctly the flow behavior. This is due to the fact that the near wall part of all turbulence models is mostly based on the physics of the ZPG boundary layer and that little is known about the physics of these APG boundary layers.

B. Near wall physics

In order to study such physics, both experimentally and numerically, it is possible to use simplified wall shapes which mimic the boundary layer behavior on the suction side of the airfoil of Fig. 8. Figure 30 gives an example of such a model designed for the boundary layer wind tunnel at LML. The boundary layer first develops on a flat plate and then, using a shaped bump, is accelerated and decelerated. The shape of the converging part of the bump should be carefully designed to avoid the development of Taylor-Görtler vortices. Most of the diverging part can be a plane, eventually with an adjustable angle, to facilitate optical access. Such a bump was first designed at LML with the help of Dassault Aviation in the frame of the AEROMEMS European research project. The objective was to perform flow control on the decelerating boundary layer. The characteristics of this boundary layer, measured by Ref. [64], are given in Fig. 28(a). Significant efforts were made to identify the physical origin of the outer peak in this experiment. They were not successful due to the difficulties of accessing the region of interest optically, to the limitations of the available characterization tool (notably in terms of time and spatial resolution) and to the nature of the physics under investigation. An Orr-Sommerfeld stability analysis of the mean velocity profile did not evidence instability.

The solution was found in a following European research project called WALLTURB, where it was possible to perform a DNS of the flow in relatively similar conditions [65]. The shape of the bump was kept identical but placed in a plane channel with fully developed turbulent channel flow as

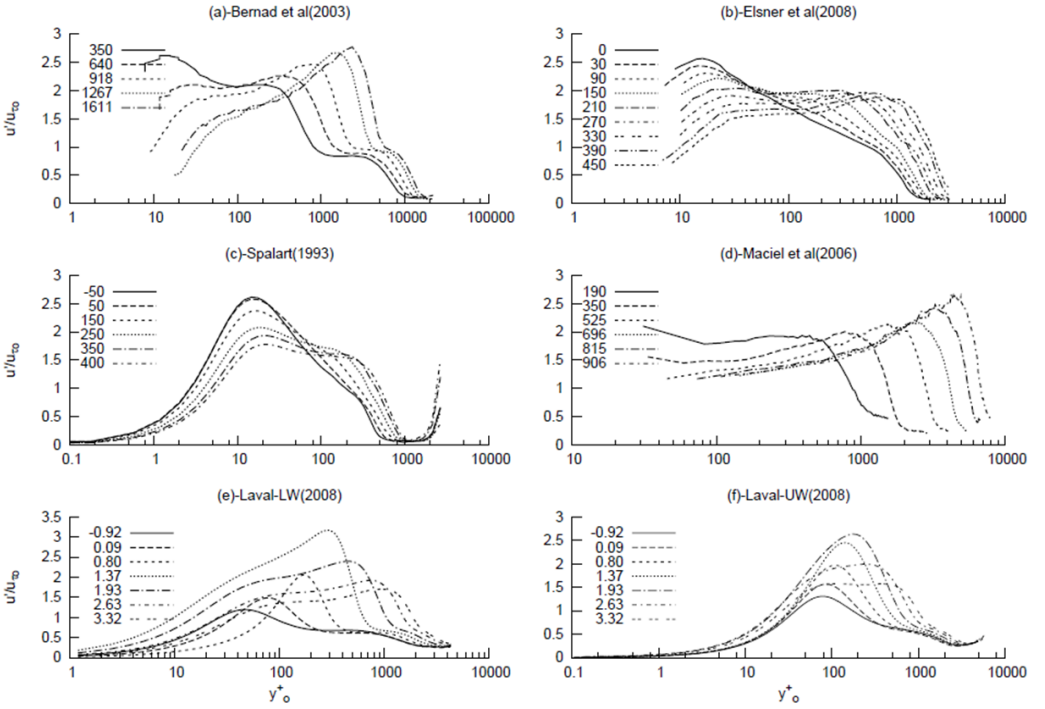

FIG. 28. Streamwise evolution of the streamwise turbulence intensity profile in a turbulent boundary layer under adverse pressure gradient from different experiments and DNS, collected by Shah *et al.* The reference velocity Uo is the external velocity at the beginning of the APG region. The wall-normal coordinate is scaled with the kinematic viscosity and the friction velocity at the beginning of the APG region. Reproduced from Ref. [61].

the upstream boundary condition. The Reynolds number of $\mathrm{Re}_\tau = 600$ was, of course, much lower than in the experiment, but sufficient to have a fully turbulent flow. Figure 31 gives an instantaneous visualization of the vortices generated in the APG region of the flow. As can be seen, there is a strong generation on the lower wall (with a very thin separation close to the wall, due to the too-low

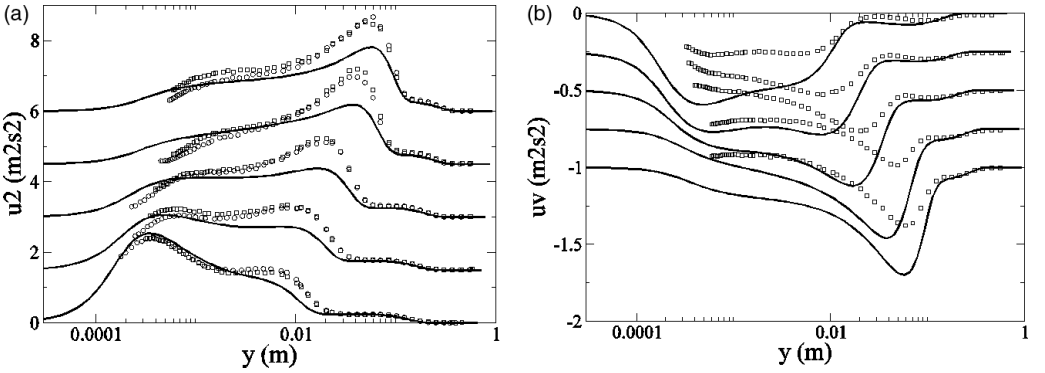

FIG. 29. Prediction of the turbulence intensity profiles in the diverging part of a converging-diverging turbulent channel flow using an EB-RSM turbulence mode [62]. Lines, model; symbols, DNS data from Marquillie *et al.*, reproduced from Ref. [63].

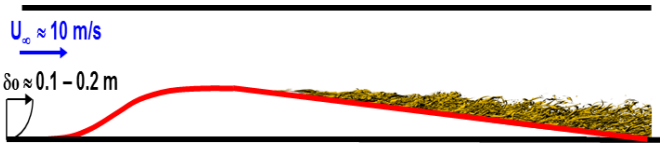

FIG. 30. Sketch of a simplified model simulating the flow on the suction side of an airfoil.

Reynolds number), but also on the upper wall where there is no separation. This is quite similar to what was observed previously in boundary layer experiments [61].

The main advantage of DNS is that all the unknowns of the Navier-Stokes equations are available at any time, everywhere, and with a very good resolution in both time and space. It is consequently possible to perform detailed analysis of the flow structure. This was done in Ref. [66] for the very near wall region. The visualization of the near wall streaks shown in Fig. 32 allowed these authors to localize the streamwise origin of the plume of vortices observed in Fig. 31. It was then possible to compute an average low-speed streak velocity profile in this region (averaging over the small black window of Fig. 32) to perform a stability analysis on this profile and to show that a varicous instability of the streaks is at the origin of the vortical plume observed downstream. This is well illustrated by Fig. 33, which shows the early development of the vortical structure originating from the instability of a low-speed streak. Here also, the mean velocity profile is not unstable. Another important result of the study of Ref. [66] was that both the sinuous and the varicous instabilities of the streaks where significantly influenced by the pressure gradient (either favorable or adverse), which means that the generation rate of vortices at the wall is linked to this parameter. This physics is, at the moment, not at all in turbulence models.

The sudden development of this instability can be partially understood by looking at Eq. (1) at the wall. At $x_2 = 0$, v_1 and v_2 are zero too and Eq. (1) reduces to

$$0 = -\frac{\partial p}{\partial x_1} + \mu \frac{\partial^2 v_1}{\partial x_2^2}. \tag{4}$$

As can be seen, a change of sign of the pressure gradient in the boundary layer immediately implies a change of sign of the second derivative of the velocity profile at the wall, that is, of the curvature of this profile. This means that an inflexion point, which is a well-known source of instability, can appear at the wall and force the mean low-speed streak profile to become unconditionally unstable.

C. Outer part behavior

As shown by Fig. 31, the varicous instability of the streaks triggered by the change of sign of the pressure gradient has a significant impact on inflexion of the outer part. An interesting question following directly is whether the near wall point of the mean velocity profile moves away from the wall downstream. This was effectively observed in Ref. [67] by looking carefully at the mean

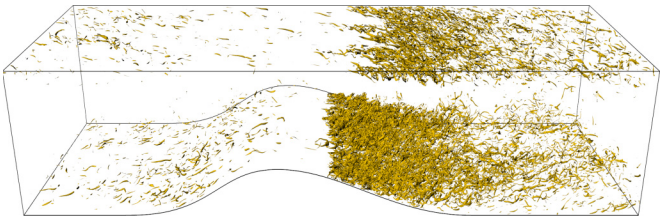

FIG. 31. Q-criterion visualization of the vortical structures generated near the wall in a DNS of converging-diverging plane channel flow, reproduced from Ref. [65].

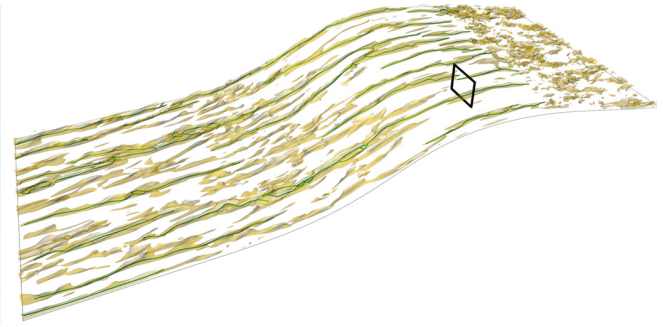

FIG. 32. Visualization of the low-speed streak generated near the wall in a DNS of converging-diverging plane channel flow, reproduced from Ref. [66]. The black frame gives the typical size of the window on which averaging of the streaks is performed.

velocity profile of the experiment of Ref. [68]. A weak inflexion point seems to appear, tightly associated to the outer turbulence peak in its movement away from the wall.

This raises critical questions about the downstream development of an APG boundary layer: How different is this boundary layer from the canonical one which is the base of turbulence models? Are the coherent structures the same? Does it present similarity properties? To answer such questions, it is necessary to develop the APG part of the flow on a distance long enough to be representative (which is not the case of most previous experiments due to technical constraints). It is also necessary to use the most advanced optical metrology to access the coherent structures. This was recently performed in a EUHIT research project coordinated by Kaehler from Bundeswehr University Munich (BUM) [69]. The experiment was performed in the boundary layer wind tunnel of LML in Lille, France. For the purpose of the experiment, a ramp model built for a previous European project (AVERT) was modified to benefit from a long APG region. The model is sketched in Fig. 34. The converging part has a contraction ratio of 0.75. It is followed by a 2.14-m-long flat plate at an angle of $+1.5^\circ$ with respect to wind tunnel floor, generating a weakly favorable pressure gradient. The last 3.5 m of the model is a flat plate set at -5° compared to the wind tunnel floor to decelerate the flow.

The streamwise pressure gradient over the entire model is given in Fig. 35. The two discontinuities in curvature at $s = 1000$ and 3500 are associated to rapid and short pressure gradient variations. The diverging part provides evidence of a significant region of nearly constant and slightly adverse pressure gradient.

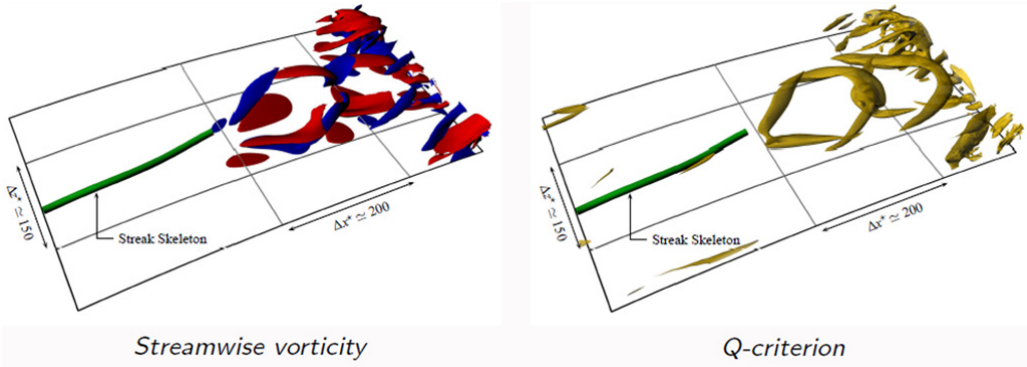

FIG. 33. Visualization of the vortical structures generated at the origin of the outer turbulence plume in a DNS of converging-diverging plane channel flow, reproduced from Ref. [66]. Left, vorticity; right, Q criterion.

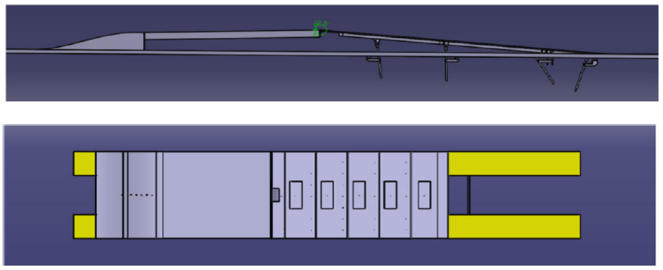

FIG. 34. APG ramp model of the EUHIT experiment, reproduced from Ref. [69].

The interest of the experiment, which is fully described in Ref. [69], is that the consortium in charge (BUM, DLR, Monash University, and LML) was able to put together enough equipment to achieve a uniquely large field of view with a good spatial resolution. By putting 16 SCMOS cameras side by side, it was possible to obtain a field of view of 3.5×0.25 m^2, giving 30 000 vector fields of 3250×238 vectors, with a spatial resolution of 2.6 mm for two free stream velocities of 5 and 9 m/s. Besides, several other measurement setups were used, based on advanced PIV approaches (see Ref. [69] for details). To illustrate the usefulness of the results, Fig. 36 gives an example of an instantaneous field of the streamwise component of the velocity fluctuations. When we compare it to Fig. 9, the similarity is evident, but the question of interest is whether these APG structures are statistically different from the ZPG ones.

In fact, as illustrated by Fig. 37 and as in the previous APG data collected [61], the one-point statistics behave quite differently from a ZPG boundary layer. A clear outer peak of turbulence develops on all Reynolds stresses [Figs. 37(a)–37(c)] while the near-wall peak of the streamwise component is still visible [Fig. 37(d)]. This should have consequences on the coherent structures characteristics. This question is under investigation by the consortium which did the experiment.

From the modeling point of view, an important issue is the possibility of self-similarity of such a boundary layer. This problem was addressed in detail by the authors of Ref. [22], who developed a similarity theory for all fully developed pressure gradient boundary layers and then showed how the scaling of Ref. [23] collapsed the velocity profiles for the developing cases, an observation explained theoretically in Ref. [70]. A subsequent publication [67] showed how this theory could

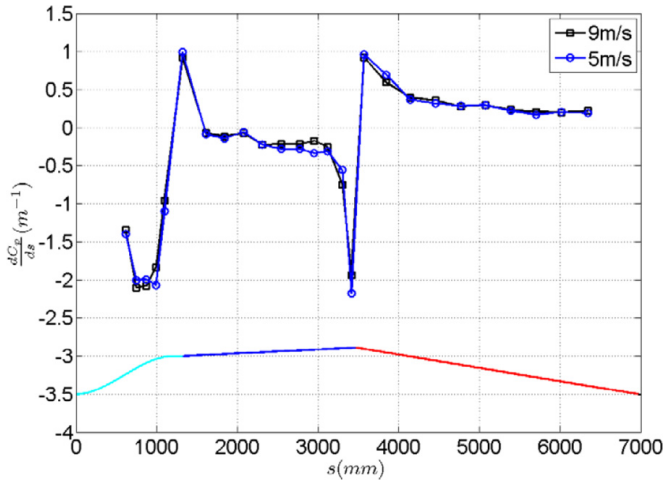

FIG. 35. Streamwise pressure gradient distribution along the EUHIT APG ramp model, reproduced from Ref. [69].

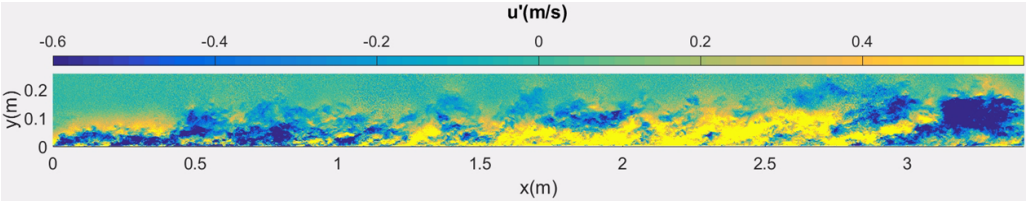

FIG. 36. Instantaneous plot of the streamwise component of the velocity fluctuations in the APG field of view of the EUHIT experiment.

be related to the outward-moving intensity peak and a developing inflexion point in the outer mean profile. Finally, researchers in Ref. [71] were even able to predict when such APG boundary layers separated. The key parameter was a new "equilibrium" parameter defined as

$$\Lambda = -\frac{\delta}{\rho U_e^2 d\delta/dx_1}\frac{dP_e}{dx_1}, \tag{5}$$

with U_e being the external velocity, dP_e/dx_1 being the pressure gradient, and δ being the boundary layer thickness at station x_1.

This Λ parameter is supposed to be constant with a value usually close to -0.2, but depending on upstream conditions [71].

Figure 38 gives the plot of the EUHIT experiment mean velocity profiles based on the scaling of Ref. [23]. Figure 39 gives the log of U_e as a function of the log of δ. Based on Eq. (5) (and using the Bernoulli equation in the free stream), the pressure gradient parameter Λ of Ref. [22] is the slope of that curve in the decreasing part, which is close to the theoretical value in this case.

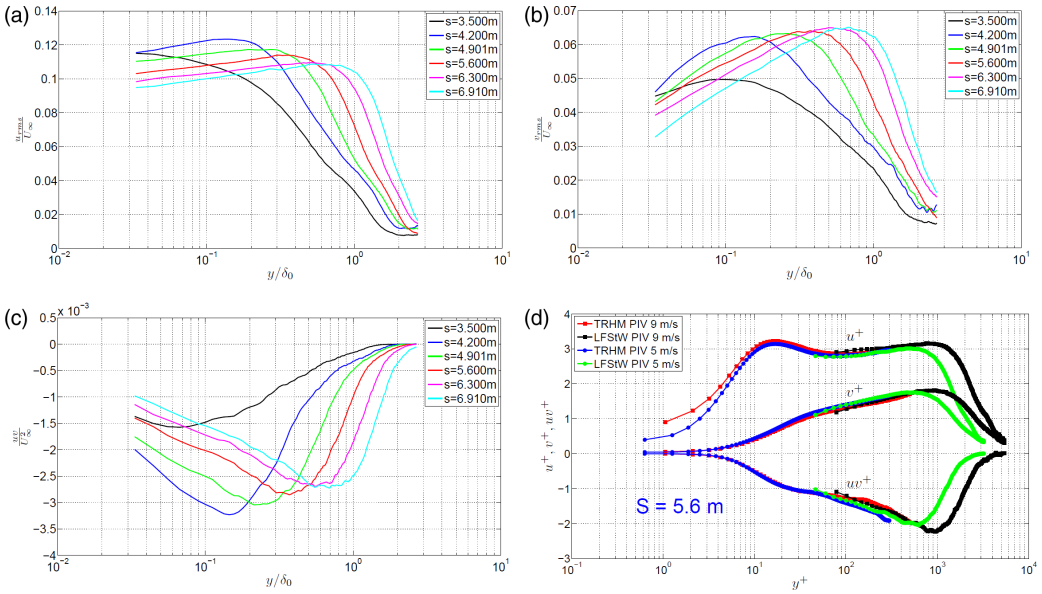

FIG. 37. Turbulence intensity profiles in the diverging part of the EUHIT experiment, measured by 2D2C PIV by Cuvier *et al.*, reproduced from Ref. [69]. (a) Streamwise turbulence intensity, (b) wall normal turbulence intensity, (c) turbulent shear stress, (d) same measurements near the wall at station $s = 5.6$ m using high-magnification time-resolved PIV [69]. Wall scaling of panel (c) is based on the local skin friction at $s = 5.6$ m, δ_0 is the boundary layer thickness at s = 1.36 m, and U_∞ the free stream velocity upstream of the ramp.

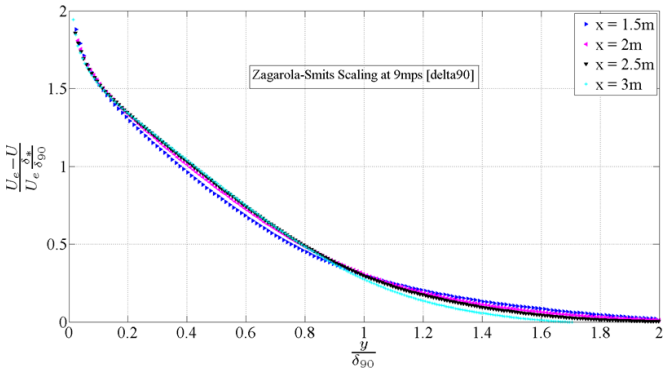

FIG. 38. Scaling of the mean velocity profile in the EUHIT experiment based on Ref. [23]. U_e, external velocity; δ^*, displacement thickness; and δ_{90}, boundary layer thick ness at 90% of U_e.

As can be seen, the agreement is fairly good in both cases, indicating that a self-similarity of this kind of boundary layer also exists.

V. DISCUSSION AND CONCLUSION

At this point, it is interesting to ask what we have learned from this new spatial information brought by both PIV and DNS. Luckily, the understanding of the phenomenon at the origin of the turbulence plume in the APG BL by Laval *et al.* [72], coupled with the analysis performed on the flat-plate boundary layer structure with PIV by Lin *et al.* [36] and the work in Ref. [49] on the outer organization, can bring some insight. Clearly, in a flat plate (or ZPG) BL, when the Reynolds number is high enough, two very similar systems of organized coherent structures exist on top of each other: one with inner scaling very close to the wall (a combination of the wall cycle of Ref. [12] and the generation mechanism of Ref. [39]) and one with outer scaling in the outer part (the very large scale motions (VLSM) evidenced in Ref. [45]). Of course, the interesting question is how these two systems interact. The action of the outer system on the near wall one was illustrated in the subsection about inner-outer crosstalk and has been clarified in Ref. [20] a few years ago: The VLSMs drive the variability of the inner system through amplitude and phase modulation. This seems to take place predominantly through large sweeping motions. These VLSMs most probably also drive the spanwise meandering of the near wall streaks as both inward and outward spanwise motions are associated with them near the wall [52]. The action of the inner system on the outer one

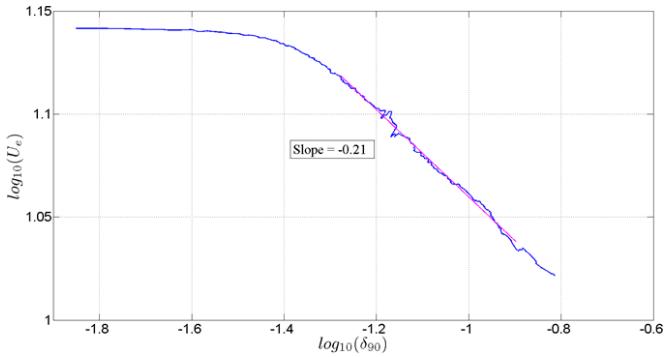

FIG. 39. Scaling of the pressure gradient in the EUHIT experiment. Following Ref. [22], the slope of the curve is the parameter Λ defined by Eq. (5).

was also illustrated in the subsection about inner-outer crosstalk and can be even more clarified by the finding of Ref. [72] regarding their APG DNS. What is the action of the adverse pressure gradient in this case? It localizes along a spanwise line (the flow is two dimensional) a continuous generation of varicous instabilities of all the low-speed streaks coming from upstream. The direct consequence is a plume of vortical structures, homogeneous in span, which propagate in the outer region over a streamwise distance of the order of a few δ. The analogy of this plume is striking with the LSM (or vortex packets) identified by Ref. [17] and the structure identified in Fig. 24. In the ZPG BL, these vortex packets find also their origin at the wall and also in a varicous instability of the streaks. But now, these instabilities (together with the associated well-known bursting process) are individual and seemingly randomly distributed over the wall surface. In fact, they are most probably triggered by the above-mentioned modulation of the near wall system by the VLSMs. As shown clearly by the spatial correlation of the streamwise velocity fluctuations (see, for example, Refs. [73,74]), they are significant structures of the outer region which develop from the wall in a manner very similar to the APG plume in the DNS of Ref. [72]. They are now individual plumes seemingly randomly localized in space and time. They carry momentum deficit, vorticity, and turbulent kinetic energy outward and interact in a nonlinear manner with the VLSM moving more quickly above them. It is probable that these LSM are mostly responsible of the observed meandering of the low- and high-momentum regions of the VLSM.

An interesting question arises then: What are the VLSMs? One should remember that they are not evidenced at low Reynolds number (no second peak of streamwise velocity fluctuations) and that a turbulent boundary layer always starts at low Reynolds number. It starts in fact by transition spots, quickly followed by instabilities of the near wall streaks. Among these instabilities, the varicous are at the origin of the first LSMs (which show some similarities with the transition spots) evidenced in the early contributions of Refs. [42,75]. When the Reynolds number increases, the velocity gradient increases also over most of the BL thickness. This means that the velocity difference between the older but still active outer LSMs coming from upstream and the new ones coming from the wall increases. This probably favors increasingly stronger interaction between them, which result in a streamwise reorganization as described by Ref. [49] and the development of the outer peak or plateau of turbulent kinetic energy (TKE). When the Reynolds number increases, the velocity gradient at the wall increases too, which means that the varicous instabilities of the streaks are probably stronger too, carrying more vorticity and turbulent shear stress away from the wall. The mean velocity gradient also increases, which means at the end that a non-negligible TKE production can exist away from the wall and be sustained by the continuous random generation of LSMs. This global scenario is, of course, partly speculative and needs complementary work to be confirmed. It nevertheless points out the fact that there is evidently a strong nonlinear and unsteady coupling between the inner and outer systems and this in both directions in what could be named a global cycle by comparison to the well-known near wall cycle.

A final remark can be made on the APG case: Why is the varicous instability fairly localized streamwise? This can probably be explained by the fact, observed in Ref. [67], that the inflexion point of the mean velocity profile, generated at the wall by the change of sign of the pressure gradient, moves outward. As the buffer layer is very thin, this inflexion point is rapidly outside of it and the varicous instability condition is not fulfilled anymore.

The aim of the present contribution was to illustrate the potential of advanced optical metrology for the assessment of turbulence physics. The access to a large amount of accurate space- and time-resolved velocity data in turbulent flows opens the way to a deeper understanding of fine physical details. An adequate combination of experimental and numerical approaches allows us to refine our insight into internal turbulence organization. From the author's point of view, for the turbulence community, this is a revolution as important as the appearance of hot wire anemometry. The progress made in the past 10 years in both optical metrology and computational fluid dynamics (CFD) allows researchers to design new approaches to the turbulence riddles. The turbulent boundary layer is not the least of these, as it is the key to fully predictive turbulence models for most flows of practical interest. At the moment, RANS models are unable to predict the outer turbulence peak,

which develops in ZPG and flat-plate boundary layers, as well as in channels and pipe flows when the Reynolds number increases. As described above, the coherent structure organization in this region of the flow becomes clearer, but the link with a near wall turbulence model has not yet been established. The fact that the near wall streak instability is sensitive to the pressure gradient is bad news for turbulence models, as this physics is not fully understood and not included in the existing models. This opens a whole field of investigation which is mandatory to address if our objective is to develop a fully predictive turbulence model, which would be very helpful to many industries. A key question is whether it will be possible to find a RANS approach to this problem. This probably calls into question the Boussinescq hypothesis, as it is clearly the production term of the turbulent energy equation which is questioned here. The near wall region appears at the moment to be the Achilles' heel of any turbulence model (including LES and lattice-Boltzmann), as it consumes most of the computer resources (which becomes prohibitive when increasing the Reynolds number) and/or is not correctly modeled. One possible track, which was under preliminary exploration in the WALLTURB EC project [76,77], is to build a low-order dynamical system able to represent sufficiently well the complexity of the near wall turbulence physics and to provide the outer turbulence model with realistic boundary conditions at a reasonable distance from the wall (of the order of 100 wall units). This is a real challenge from the theoretical, mathematical, experimental, and CFD point of view as such a model does not exist at the moment. Moreover, as clearly shown by the above analysis, it cannot just live by itself but must be coupled to the outer model in both directions (in and out). The tools are nevertheless available and mature enough today for young researchers to open the way to such a challenging objective.

ACKNOWLEDGMENTS

The author is particularly thankful to the Region Nord Pas de Calais for continuous financial support, notably through the CISIT program. He would also like to acknowledge the contribution of his colleagues, Patrick Dupont, Jean Marc Foucaut, and Jean Philippe Laval. He would definitely like to thank Bill George for fruitful discussions about turbulence and detailed proof reading of this manuscript. Finally, he would like to acknowledge Woutijn J. Baars for his enlightening presentation at the Wall Turbulence Workshop in Lille on June 16, 2017.

[1] H. H. Fernholdz and P. J. Finley, The incompressible zero-pressure-gradient boundary layer: An assessment of the data, Prog. Aerospace Sci. **32**, 245 (1996).

[2] A. J. Smits and I. Marusic, High Reynolds number wall turbulence, Annu. Rev. Fluid Mech. **43**, 353 (2011).

[3] M. Vallikivi, M. Hultmark, and A. J. Smits, Turbulent boundary layer statistics at very high Reynolds numbers, J. Fluid Mech. **779**, 371 (2015).

[4] P. Vincenti, J. Klewicki, C. Morrill-Winter, C. M. White, and M. Wosnik, Streamwise velocity statistics in turbulent boundary layers that spatially develop to high Reynolds number, Exp. Fluids **54**, 1 (2013).

[5] J. Carlier and M. Stanislas, Experimental study of eddy structures in a turbulent boundary layer using particle image velocimetry, J. Fluid Mech. **535**, 143 (2005).

[6] P. S. Klebanoff, Characteristics of turbulence in a boundary layer with zero pressure gradient, NACA **1247**, 1135 (1955).

[7] L. P. Erm and P. N. Joubert, Low-Reynolds-number turbulent boundary layers, J. Fluid Mech. **230**, 1 (1991).

[8] P. Spalart, Direct simulation of a turbulent boundary layer up to $\mathrm{Re}_\theta = 1410$, J. Fluid Mech. **187**, 61 (1988).

[9] T. Theodorsen, Mechanism of turbulence, in *Proceedings of the Midwest Conference in Fluid Mechanics*, 2nd ed. (Ohio State University, Columbus, OH, 1952), p. 1.

[10] S. J. Kline, W. C. Reynolds, F. A. Schraub, and P. W. Runstadl, Structures of turbulent boundary layers, J. Fluid Mech. **30**, 741 (1967).
[11] E. R. Corino and R. S. Brodkey, A visual investigation of the wall region in turbulent flow, J. Fluid Mech. **37**, 1 (1969).
[12] H. T. Kim, S. J. Kline, and W. C. Reynolds, The production of turbulence near a smooth wall in a turbulent boundary layers, J. Fluid Mech. **50**, 133 (1971).
[13] J. Kim, On the structure of wall-bounded turbulent flows, Phys. Fluids **26**, 2088 (1983).
[14] J. Kim and P. Moin, The structure of the vorticity field in turbulent channel flow, part 2: Study of ensemble averaged fields, J. Fluids Mech. **162**, 339 (1986).
[15] R. F. Blackwelder and R. E. Kaplan, On the wall structure of the turbulent boundary layer, J. Fluid Mech. **76**, 89 (1976).
[16] J. M. Hamilton, J. Kim, and F. Waleffe, Regeneration mechanisms of near-wall turbulence structures, J. Fluid Mech. **287**, 317 (1995).
[17] R. J. Adrian, C. D. Meinhart, and C. D. Tomkins, Vortex organization in the outer layer of the turbulent boundary layer, J. Fluid Mech. **422**, 1 (2000).
[18] M. Hultmark, M. Vallikivi, S. C. C. Bailey, and A. J. Smits, Turbulent Pipe Flow at Extreme Reynolds Numbers, Phys. Rev. Lett. **108**, 094501 (2012).
[19] I. Marusic, B. J. Mackeon, P. Monkewitz, H. M. Nagib, A. J. Smits, and K. R. Sreenivasan, Wall-bounded turbulent flows at high Reynolds numbers: Recent advances and key issues, Phys. Fluids **22**, 065103 (2010).
[20] I. Marusic, R. Mathis, and N. Hutchins, Predictive model for wall-bounded turbulent flow, Science **329**, 193 (2010).
[21] N. Hutchins and I. Marusic, Evidence of very long meandering features in the logarithmic region of turbulent boundary layers, J. Fluid Mech. **579**, 1 (2007).
[22] L. Castillo and W. K. George, Similarity analysis for turbulent boundary layers with pressure gradient: Outer flow, AIAA J. **39**, 41 (2001).
[23] M. V. Zaragola and A. J. Smits, Mean-flow scaling of turbulent pipe flow, J. Fluid Mech. **373**, 33 (1998).
[24] C. E. Willert and M. Gharib, Digital particle image velocimetry, Exp. Fluids **10**, 181 (1991).
[25] S. Srinath, J. C. Vassilicos, C. Cuvier, J.-P. Laval, M. Stanislas, and J.-M. Foucaut, Attached flow structure and streamwise energy spectra in a turbulent boundary layer, J. Fluid Mech. (to be published).
[26] M. Vallikivi, B. Ganapathissubramani, and A. J. Smits, Spectral scaling in boundary layers and pipes at very high Reynolds numbers, J. Fluid Mech. **771**, 303 (2014).
[27] I. Marusic, R. Mathis, and N. Hutchins, High Reynolds number effects in wall turbulence, Int. J. Heat Fluid Flow **31**, 418 (2010).
[28] M. Raffel, C. Willert, and J. Kompenhans, *Particle Image Velocimetry* (Springler-Verlag, Berlin, 1998).
[29] F. Scarano, Tomographic PIV: Principles and practice, Meas. Sci. Technol. **24-1**, 012001 (2013).
[30] D. Schanz, A. Schroder, S. Gesemann, D. Michaelis, and B. Wieneke, "Shake the box": A highly efficient and accurate tomographic particle tracking velocimetry (TOMO-PTV) method using prediction of particle positions, in *10th International Symposium on Particle Image Velocimetry—PIV13*, Delft, The Netherlands (2010).
[31] W. K. George and L. Castillo, Zero-pressure-gradient turbulent boundary layer, Appl. Mech. Rev. **50**, 689 (1997).
[32] P. A. Monkewitz, K. A. Chauman, and H. M. Nagib, Comparison of mean flow similarity laws in zero pressure gradient turbulent boundary layers, Phys. Fluids **20**, 105102 (2008).
[33] R. Panton, *Self-Sustaining Mechanisms of Wall Turbulence*, Advances in Fluid Mechanics (Computational Mechanics, 1997).
[34] W. K. George, Is there a universal log law for turbulent wall-bounded flows? Philos. Trans. R. Soc. London, Ser. A **365**, 789 (2007).
[35] J. Lin, Etude détaillée des structures cohérentes de la zone tampon de la turbulence de paroi à l'aide de données de PIV stéréoscopique, Ph.D. thesis n°28, Ecole Centrale de Lille, Lille, France, 2006.
[36] J. Lin, J.-P. Laval, J.-M. Foucaut, and M. Stanislas, Quantitative characterization of coherent structures in the buffer layer of near-wall turbulence. Part 1: Streaks, Exp. Fluids **45**, 999 (2008).

[37] C. R. Smith and S. P. Metzler, The characteristics of low speed streaks in the near wall region of a turbulent boundary layer, J. Aeronaut. Sci. **129**, 27 (1983).
[38] S. Herpin, M. Stanislas, J. M. Foucaut, and S. Coudert, Influence of the Reynolds number on the vortical structures in the logarithmic region of turbulent boundary layers, J. Fluid Mech. **716**, 5 (2013).
[39] W. Schoppa and F. Hussain, Coherent structure generation in near wall turbulence, J. Fluid Mech. **453**, 57 (2002).
[40] F. Waleffe, On a self-sustaining process in shear flows, Phys. Fluids **9**, 883 (1997).
[41] J.-P. Laval, W. Elsner, L. Kuban, and M. Marquillie, LES modeling of converging diverging turbulent channel flow, in *Progress in Wall Turbulence: Understanding and Modelling*, ERCOFTAC series, edited by M. Stanislas, J. Jimenez, and I. Marusic (Springer, Villeneuve d'Ascq, France, 2009), p. 355.
[42] M. R. Head and P. Bandyopadhyay, New aspect of turbulent boundary-layer structure, J. Fluid Mech. **107**, 297 (1981).
[43] Y. Wu and K. T. Chritensen, Population trends of spanwise vortices in wall turbulence, J. Fluid Mech. **568**, 55 (2006).
[44] K. C. Kim and R. J. Adrian, Very large-scale motion in the outer layer, Phys. Fluids **11**, 417 (1999).
[45] B. J. Balakumar and R. J. Adrian, Large- and very-large-scale motions in channel and boundary-layer flows, Philos. Trans. R. Soc. London, Ser. A **365**, 665 (2007).
[46] B. Ganapathisubramani, N. T. Clemens, and D. S. Dolling, Large-scale motions in a supersonic turbulent boundary layer, J. Fluid Mech. **556**, 271 (2006).
[47] J. Delville, P. Braud, S. Coudert, J.-M. Foucaut, C. Fourment, W. K. George, P. B. V. Johansson, J. Kostas, F. Mehdi, A. Royer, M. Stanislas, and M. Tutkun, The WALLTURB joined experiment to assess the large scale structures in a high Reynolds number turbulent boundary layer, in *Progress in Wall Turbulence: Understanding and Modelling*, ERCOFTAC series, edited by M. Stanislas, J. Jimenez, and I. Marusic (Springer, Villeneuve d'Ascq, France, 2009).
[48] R. Dekou, Large scale organization of wall turbulence, Ph.D. thesis n°295, Thèse de l'Ecole Centrale de Lille, Lille, France, 2016.
[49] R. Dekou, J. M. Foucaut, S. Roux, M. Stanislas, and J. Delville, Large scale organization of a near wall turbulent boundary layer, Int. J. Heat Fluid Flow **61A**, 12 (2016).
[50] R. J. Adrian and P. Moin, Stochastic estimation of organized turbulent structures: Homogeneous shear-flow, J. Fluid Mech. **190**, 531 (1988).
[51] J. C. del Álamo, J. Jiménez, P. Zandonade, and R. D. Moser, Self-similar vortex clusters in the logarithmic region, J. Fluid Mech. **561**, 329 (2006).
[52] Y. Naka, M. Stanislas, J.-M. Foucaut, S. Coudert, J.-P. Laval, and S. Obi, Space-time pressure-velocity correlation in a turbulent boundary layer, J. Fluid Mech. **771**, 624 (2014).
[53] J. C. Vassilicos, J.-P. Laval, J.-M. Foucaut, and M. Stanislas, The streamwise turbulence intensity in the intermediate layer of turbulent pipe flow, J. Fluid Mech. **774**, 324 (2015).
[54] A. E. Perry, S. Henbest, and M. S. Chong, A theoretical and experimental study of wall turbulence, J. Fluid Mech. **165**, 163 (1986).
[55] J.-P. Laval, J.-C. Vassilicos, J.-M. Foucaut, and M. Stanislas, Comparison of turbulence profiles in high-Reynolds-number turbulent boundary layers and validation of a predictive model, J. Fluid Mech. **814**, R2 (2017).
[56] N. Hutchins, C. Kapil, I. Marusic, J. Monty, and J. Klewicki, Towards reconciling the large-scale structure of turbulent boundary layers in the atmosphere and laboratory, Boundary-Layer Meteorol. **145**, 273 (2012).
[57] M. M. Metzger, B. J. McKeon, and H. Holmes, The near-neutral atmospheric surface layer: Turbulence and non-stationarity, Philos. Trans. R. Soc. London, Ser. A **365**, 859 (2007).
[58] W. P. Jones and B. E. Launder, The prediction of laminarization with a two-equation model of turbulence, Int. J. Heat Mass Transfer **15**, 301 (1972).
[59] P. R. Spalart and J. H. Watmuff, Experimental and numerical investigation of a turbulent boundary layer with pressure gradients, J. Fluid Mech. **249**, 337 (1993).
[60] M. Skote and D. S. Henningson, Direct numerical simulation of separating turbulent boundary layers, J. Fluid Mech. **471**, 107 (2002).

[61] S. I. Shah, M. Stanislas, and J.-P. Laval, A specific behavior of adverse pressure gradient near wall flows, in *Progress in Wall Turbulence: Understanding and Modelling*, ERCOFTAC series Vol. 14, edited by M. Stanislas, J. Jimenez, and I. Marusic (Springer, Villeneuve d'Ascq, France, 2010), p. 257.

[62] R. Manceau, Recent progress in the development of the elliptic blending Reynolds-stress model, Int. J. Heat Fluid Fl. **51**, 195 (2015).

[63] M. Marquillie, J.-P. Laval, and R. Dolganov, Direct numerical simulation of separated channel flows with a smooth profile, J. Turbulence **9-1**, 1 (2008).

[64] A. Bernard, J. M. Foucaut, P. Dupont, and M. Stanislas, Decelerating boundary layer: A new scaling and mixing length model, AIAA J. **41**, 248 (2003).

[65] J.-P. Laval and M. Marquillie, Direct numerical simulations of converging-diverging channel flow, in *Progress in Wall Turbulence: Understanding and Modelling*, ERCOFTAC series, edited by M. Stanislas, J. Jimenez, and I. Marusic (Springer, Villeneuve d'Ascq, France, 2009), p. 203.

[66] M. Marquillie, U. Ehrenstein, and J.-P. Laval, Instability of streaks in wall turbulence with adverse pressure gradient, J. Fluid Mech. **681**, 205 (2011).

[67] M. Stanislas, W. K. George, and J.-P. Laval, New insights into adverse pressure gradient boundary layers, in *Progress in Turbulence and Wind Energy: Proceeding of the iTi Conference in Turbulence 2010* (Bertinoro, Italy, 2010), p. 201.

[68] P. E. Skåre and P.-Å Krogstad, A turbulent boundary layer near separation, J. Fluid Mech. **272**, 319 (1994).

[69] C. Cuvier, S. Srinath, M. Stanislas, J. M. Foucaut, J. P. Laval, C. J. Kähler, R. Hain, S. Scharnowski, A. Schröder, R. Geisler *et al.*, Extensive characterization of a high reynolds number decelerating boundary layer using advanced optical metrology, J. Turbulence **18**, 1 (2017).

[70] M. Wosnik and W. K. George, Reconciling the Zagarola/Smits scaling with the George/Castillo theory for the zero pressure gradient turbulent boundary layer, in *Proceedings of the 38th Aerospace Sciences Meeting and Exhibit, Aerospace Sciences Meetings* (AIAA, Reston, VA, 2010).

[71] L. Castillo, X. Wang, and W. K. George, Similarity analysis for turbulent boundary layers with pressure gradient: Outer flow, J. Fluids Eng. **126**, 297 (2004).

[72] J.-P. Laval, M. Marquillie, and U. Ehrenstein, Low speed streaks instability of direct numerical simulation of turbulent boundary layer flows with adverse pressure gradient, in *Proceedings of the Seventh International Symposium on Turbulence and Shear Flow Phenomena (TSFP-7)* (Ottawa, Canada, 2011).

[73] J.-M. Foucaut, S. Coudert, M. Stanislas, J. Delville, M. Tutkun, and W. K. George, Spatial correlation from the SPIV database of the Wallturb experiment, in *Progress in Wall Turbulence: Understanding and Modelling*, ERCOFTAC series, edited by M. Stanislas, J. Jimenez, and I. Marusic (Springer, Villeneuve d'Ascq, France, 2009).

[74] M. Tutkun, W. K. George, J. Delville, M. Stanislas, P. B. V. Johansson, J.-M. Foucaut, and S. Coudert, Two-point correlations in high Reynolds number flat plate turbulent boundary layers, J. Turbulence **10**, 1 (2009).

[75] R. E. Falco, Coherent motions in the outer region of turbulent boundary layers, Phys. Fluids **20**, S124 (1977).

[76] G. Lehnasch, J. Jouanguy, J.-P. Laval, and J. Delville, Pod based ROM for prescribing turbulent near wall unsteady boundary conditions, in *Progress in Wall Turbulence: Understanding and Modelling*, ERCOFTAC series, edited by M. Stanislas, J. Jimenez, and I. Marusic (Springer, Villeneuve d'Ascq, 2009).

[77] B. Podvin, A pod-based model for the turbulent wall layer, in *Progress in Wall Turbulence: Understanding and Modelling*, ERCOFTAC series, edited by M. Stanislas, J. Jimenez, and I. Marusic (Springer, Villeneuve d'Ascq, France, 2009).